Journal for ImmunoTherapy of Cancer

Selective IL-1 activity on CD8$^+$ T cells empowers antitumor immunity and synergizes with neovasculature-targeted TNF for full tumor eradication

Bram Van Den Eeckhout ,[1,2] Leander Huyghe ,[1,2] Sandra Van Lint ,[1,2] Elianne Burg,[1,2] Stéphane Plaisance ,[3] Frank Peelman ,[1,2] Anje Cauwels ,[1,2] Gilles Uzé ,[4] Niko Kley,[5] Sarah Gerlo ,[1,2] Jan Tavernier [1,2,5]

To cite: Van Den Eeckhout B, Huyghe L, Van Lint S, *et al*. Selective IL-1 activity on CD8$^+$ T cells empowers antitumor immunity and synergizes with neovasculature-targeted TNF for full tumor eradication. *Journal for ImmunoTherapy of Cancer* 2021;**9**:e003293. doi:10.1136/jitc-2021-003293

► Additional supplemental material is published online only. To view, please visit the journal online (http://dx.doi.org/10.1136/jitc-2021-003293).

LH and SVL contributed equally.

SG and JT are joint senior authors.

Accepted 17 October 2021

[1]VIB-UGent Center for Medical Biotechnology, Ghent, Belgium
[2]Department of Biomolecular Medicine, Ghent University, Ghent, Belgium
[3]VIB Nucleomics Core, Leuven, Belgium
[4]IRMB, University Montpellier, INSERM, CNRS, Montpellier, France
[5]Orionis Biosciences Inc, Waltham, Massachusetts, USA

Correspondence to
Prof. Dr. Jan Tavernier; jan.tavernier@vib-ugent.be

Prof. Dr. Sarah Gerlo; sarah.gerlo@ugent.be

ABSTRACT

Background Clinical success of therapeutic cancer vaccines depends on the ability to mount strong and durable antitumor T cell responses. To achieve this, potent cellular adjuvants are highly needed. Interleukin-1β (IL-1β) acts on CD8$^+$ T cells and promotes their expansion and effector differentiation, but toxicity and undesired tumor-promoting side effects hamper efficient clinical application of this cytokine.

Methods This 'cytokine problem' can be solved by use of AcTakines (Activity-on-Target cytokines), which represent fusions between low-activity cytokine mutants and cell type-specific single-domain antibodies. AcTakines deliver cytokine activity to *a priori* selected cell types and as such evade toxicity and unwanted off-target side effects. Here, we employ subcutaneous melanoma and lung carcinoma models to evaluate the antitumor effects of AcTakines.

Results In this work, we use an IL-1β-based AcTakine to drive proliferation and effector functionality of antitumor CD8$^+$ T cells without inducing measurable toxicity. AcTakine treatment enhances diversity of the T cell receptor repertoire and empowers adoptive T cell transfer. Combination treatment with a neovasculature-targeted tumor necrosis factor (TNF) AcTakine mediates full tumor eradication and establishes immunological memory that protects against secondary tumor challenge. Interferon-γ was found to empower this AcTakine synergy by sensitizing the tumor microenvironment to TNF.

Conclusions Our data illustrate that anticancer cellular immunity can be safely promoted with an IL-1β-based AcTakine, which synergizes with other immunotherapies for efficient tumor destruction.

BACKGROUND

CD8$^+$ T cells are pivotal players in anticancer immunity.[1] Many cancer immunotherapies, therefore, focus on revitalizing CD8$^+$ T cell responses, for example, by interfering with pathways of T cell inhibition.[2] Unfortunately, immune checkpoint inhibitors are only effective in subsets of patients and additional interventions are required when responsiveness is limited or absent.[3] Moreover, initially responsive patients will often develop acquired resistance to therapy.[4] Checkpoint inhibitors are currently evaluated in combination with other strategies, including cancer vaccination and adoptive T cell transfer (ATCT).[5–11] Yet, the efficacy of these strategies remains relatively low and they could benefit from codelivery of so-called 'cellular' adjuvants that improve the expansion, function and peripheral survival of both endogenously generated and adoptively transferred CD8$^+$ T cells.[12]

A promising candidate for a cellular adjuvant is the proinflammatory cytokine interleukin-1β (IL-1β),[13] which empowers proliferation, effector functionality and memory differentiation of CD8$^+$ T cells in different experimental models.[14–17] Recently, Lee *et al*. demonstrated that repeated delivery of wild-type (WT) IL-1β in mice with established B16 melanomas improves the antitumor effect of ATCT by enhancing the formation of tumor-associated antigen (TAA)-specific effector CD8$^+$ T cells and their peripheral trafficking and survival.[18] Despite these promising results, two major hurdles hamper clinical translation of IL-1 activity. First, systemic delivery of WT IL-1β induces damaging toxicities, with maximum tolerated doses calculated from phase I clinical trials ranging from 0.07 to 0.3 µg/kg body weight. This toxicity is dose-dependent and includes influenza-like symptoms at lower doses and cardiovascular issues upon administration of higher amounts of WT IL-1β.[19] Second, chronic inflammation in the tumor microenvironment (TME) can promote cancer progression and as a major inflammatory mediator, the protumorigenic properties of IL-1β are increasingly recognized.[20] IL-1β fuels tumor development by a plethora of different mechanisms, including

promotion of angiogenesis, metastasis and formation of an immunosuppressive TME, characterized by accumulation of $CD11b^+Gr\text{-}1^+$ myeloid-derived suppressor cells and $CD11b^+Ly6G^+$ neutrophils that can both dampen $CD8^+$ T cell immunity.[21–24]

Importantly, these limitations stem from IL-1β's pleiotropic mode of action.[13] Selective delivery of IL-1β activity to $CD8^+$ T cells might limit toxicity and undesired side effects, hence allowing application as a cellular adjuvant in cancer immunotherapy. Selective cytokine activity can be achieved using AcTakines ('Activity-on-Target cytokines'), which are fusion proteins comprizing a cytokine mutant with reduced receptor affinity and a single-domain antibody (sdAb) directed towards a cell type-specific surface molecule. AcTakines remain inactive *en route* through the body and regain full activity on target cell binding.[25] Previously, we reported on the development of an AcTakine that targets activity of the IL-1β Q148G mutant to $CD8^+$ T cells (CD8α AcTaleukin-1/ALN-1) in an influenza A model.[26]

Here, we demonstrate that CD8α ALN-1 drives antitumor $CD8^+$ T cell responses in subcutaneous (s.c.) melanoma (B16) and Lewis lung carcinoma (LLC) models. The potent cellular adjuvant effect of CD8α ALN-1 empowers epitope spreading, expansion and effector functionality of endogenous host T cells and enhances the efficacy of ATCT. CD8α ALN-1 synergizes with a neovasculature-targeted tumor necrosis factor (TNF) AcTakine, leading to complete tumor destruction and formation of immunological memory that protects against secondary tumor challenge. Hence, selective IL-1β activity on $CD8^+$ T cells provides a safe way to promote a diverse antitumor T cell response and synergy with other immunotherapies.

METHODS

Tumor models

Mice were inoculated s.c. in the shaved back with 0.5×10^6 tumor cells in 50 µL of PBS (14190–169, Thermo Fisher Scientific) under mild isoflurane anesthesia (Abbott Animal Health). Mice were sacrificed when both perpendicular tumor sides exceeded 10 mm or when 20% reduction in starting body weight was observed.

Flow cytometry and antibodies

Tissues were collected in PBS and mechanically mashed on 70 µm nylon strainers. Spleens and tumors were treated with a home-made red blood cell lysis buffer (155 mM Na_4Cl, 12 mM $NaHCO_3$ and 127 µM EDTA in PBS *p*H 7.4). Single cell suspensions were incubated for 30 min at 4°C in PBS with anti-mouse CD16/32 to block Fc receptors. Staining was performed for 1 hour at 4°C with antibodies or dye diluted in PBS (see online supplemental table 1). Sample fixation and permeabilization was performed using the Foxp3 Transcription Factor Staining Buffer Set (00-5523-00, Thermo Fisher Scientific). Cells were recorded on a four-laser Attune Nxt flow cytometer (Thermo Fisher Scientific) or sorted on a three-laser FACSAria II (BD Biosciences). Data were analyzed using FlowJo software (Treestar).

Adoptive T cell transfer

OT-I $CD8^+$ T cells were purified from spleens by negative selection magnetic-activated cell sorting (130-104-075, Miltenyi Biotec). For proliferation experiments, OT-I $CD8^+$ T cells were labeled with 5 µM CTV (C34557, Thermo Fisher Scientific). 0.5×10^6 OT-I $CD8^+$ T cells in 200 µL PBS were intravenously (i.v.) transferred.

Anti-SIINFEKL cytotoxicity and anti-interferon-γ ELISpot assay

Splenocytes were suspended in RPMI-1640 + 10% FBS. Half of the splenocytes were pulsed with SIINFEKL (ovalbumin, $OVA_{257–264}$) (10 µg/mL) (AS-60 193-1, AnaSpec) for 2 hour at 37°C, 5% CO_2 and remaining cells were left unloaded. Cells loaded with SIINFEKL were labeled with 5 µM CTV and unloaded cells were labeled with 500 nM CTV. Splenocytes were pooled 1:1 and transferred i.v. (10^7 cells/mouse in 200 µL PBS). Tumor-draining lymph nodes (TDLNs) from recipient mice were processed to single cells and seeded (2.5×10^5 cells/well) for 72 hours in RPMI-1640 + 10% FBS+SIINFEKL peptide (5 µg/mL) in a 96-well plate, precoated overnight (4°C) with anti-interferon-γ (IFN-γ) antibody (CT317-T2, U-CyTech Biosciences). ELISpots were developed according to the manufacturer's instructions and the remainder of cells was recorded via flow cytometry.

Antibodies in depletion and inhibition *in vivo* experiments

For depletion of $CD8^+$ T cells, 250 µg of anti-mouse CD8α monoclonal antibody (clone YTS 169.4, BP0117, Bio-Connect) was intraperitoneally (i.p.) administered. For inhibition of IFN-γ activity, 500 µg of a neutralizing anti-mouse IFN-γRI monoclonal antibody (clone GR-20, BE0029, Bio-Connect) was i.p. administered.

$CD8^+$ T cell sorting and RNA isolation

$CD8^+$ T cells were sorted (4°C) from mixed cell populations and captured in RLT Plus lysis buffer + β-mercaptoethanol. RNA was isolated following the manufacturer's instructions (RNeasy Plus Micro Kit, 74034, Qiagen). Concentration, quality and RNA integrity was assessed using an Agilent 2100 Bioanalyzer (Agilent). Samples with RIN ≥8 and 280/260 and 260/230 values>1.8 were used for library preparation.

T cell receptor sequencing, data processing and analysis

The sequencing library was constructed using the Qiagen QIAseq Mouse T cell receptor (TCR) Panel Immune Repertoire RNA Library Kit (Qiagen) according to the manufacturer's instructions. More detail can be found in online supplemental methods.

Ex vivo restimulation for detection of intracellular cytokine production

Splenocytes were suspended in RPMI-1640 + 10% FBS + SIINFEKL peptide (10 µg/mL) and incubated for 2 hours at 37°C, 5% CO_2. After 2 hours, brefeldin A solution

(1000x) (00-4506-51, Thermo Fisher Scientific) was added and samples were further incubated at 37°C, 5% CO_2 overnight.

Multiplex cytokine analysis

Blood was sampled from the tail vein, collected in EDTA-coated microcuvette tubes (Sarstedt) and centrifuged at 14000xg for 10 min at 4°C. Cytokine and chemokine concentrations were determined with the Cytokine and Chemokine Convenience 36-Plex Mouse ProcartaPlex Panel 1A (EPXR360-26092-901, Thermo Fisher Scientific) following the manufacturer's instructions.

Statistical analyses and data presentation

Statistical analyses were performed using the GraphPad Prism V.9 software (GraphPad Software). Data are presented as mean ± SEM in all experiments, unless stated otherwise. The number of independent biological replicates or the number of individual mice has been indicated as '*n*'. Statistical significance was throughout defined as $p<0.05$. More detail can be found in online supplemental methods.

RESULTS

A therapeutic cancer vaccine supplemented with CD8α ALN-1 slows down tumor growth without evoking systemic toxicity

We first assessed the efficacy and safety of a cancer vaccine adjuvanted with CD8α ALN-1. In order to obtain this AcTakine, we first introduced the Q148G mutation in human IL-1β, which renders a cytokine with low biological activity that can be completely restored on its delivery by a high-affinity sdAb.[26] Mice with s.c. inoculated LLC that stably expresses the OVA model antigen (LLC-OVA) were treated i.p. with PBS or OVA, either alone or combined with WT IL-1β, CD8α ALN-1 or untargeted BcII10 ALN-1 (figure 1A,B). Treatment with OVA + CD8α ALN-1 caused a significant delay in tumor growth over the treatment period (figure 1C,D), however, tumor control was transient and volumes rapidly caught up with lesion sizes observed in controls on treatment discontinuation. Importantly, this effect depended on CD8α targeting, as neither treatment with WT IL-1β or BcII10 ALN-1 had antitumor effect. Repeated administration of CD8α ALN-1 was free of measurable toxicity, whereas equivalent amounts of WT IL-1β caused body weight loss and gravely impacted the well-being of mice (figure 1E). Systemic delivery of CD8α ALN-1 can thus safely delay tumor growth over the treatment period by targeting $CD8\alpha^+$ cells.

The antitumor effect of CD8α ALN-1 depends on activation of the endogenous $CD8^+$ T cell response

Next, we studied the $CD8^+$ T cell response in the TDLN and LLC-OVA tumor tissue after treatment (figure 2A). While we did not find statistically significant differences in the relative amount of $CD8^+$ T cells in the TDLN, mice treated with OVA + CD8α ALN-1 showed reduced frequencies of naive $CD8^+$ T cells compared with controls (figure 2B, see online supplemental figure 1A for the gating strategy). Accordingly, this corresponded with an increase in the relative amount of effector $CD8^+$ T cells. In tumors, treatment with OVA + CD8α ALN-1 caused an increase in the fraction of $CD8^+$ T cells, a decrease of naive $CD8^+$ T cells and higher frequencies of effector $CD8^+$ T cells compared with controls (figure 2C, see online supplemental figure 1B for the gating strategy).

We then measured the capacity of $CD8^+$ T cells to release IFN-γ after *ex vivo* restimulation with TAA and kill target cells in vivo (figure 2D). Upon *ex vivo* restimulation of TDLN cells with SIINFEKL ($OVA_{257-264}$), we recorded more IFN-γ release after treatment with OVA + CD8α ALN-1 (figure 2E). Concomitantly, we observed enhanced specific cytolytic activity in mice treated with OVA + CD8α ALN-1 (figure 2F, see online supplemental figure 2 for the gating strategy). Collectively, treatment with CD8α ALN-1 stimulates host $CD8^+$ T cells in the TDLN and tumor to acquire a favorable effector phenotype and execute effector functionality in response to TAA encounter.

We analyzed the importance of $CD8^+$ T cells in the CD8α ALN-1-mediated antitumor effect by depletion of cytotoxic T lymphocytes (CTLs) prior to and during treatment. The partial control over tumor growth on treatment with OVA + CD8α ALN-1 was completely lost on CTL depletion (figure 2G). Again, repeated delivery of CD8α ALN-1 was not associated with measurable toxicity (figure 2H). These data demonstrate the necessity of $CD8^+$ T cells during the antitumor response initiated by CD8α ALN-1.

TCR repertoire analysis reveals increased host CTL diversity induced by CD8α ALN-1

We assessed whether treatment with CD8α ALN-1 mediates clonal expansion of host T cells. We first used a method that detects changes in murine TCR repertoires via flow cytometry-based TCR Vβ analysis (figure 3A, see online supplemental figure 3 for the gating strategy).[27] Treatment with OVA + CD8α ALN-1 caused significant, although modest, changes in frequencies of different $CD8^+$ T cell TCR Vβ clonotypes (Vβ5.1/2 and Vβ11) compared with OVA alone (figure 3B). Of note, decrease of the dominant TCR Vβ5.1/2 clonotype was compensated by small increases in various other clonotypes (including TCR Vβ9, Vβ11, Vβ13 and Vβ14; summarized in online supplemental table 2) that did not reach statistical significance.

Next, we performed TCR sequencing to investigate effects on the T cell repertoire in more depth. We sorted $CD8^+$ T cells from the TDLN and LLC-OVA tumor of mice treated with PBS, OVA alone or OVA + CD8α ALN-1 and isolated RNA for bulk TCR sequencing (figure 3A, see online supplemental figure 4A and B for the gating strategies). Host TCRB sequences in TDLN revealed clear expansion of numerous $CD8^+$ T cell clones after treatment with OVA + CD8α ALN-1 (figure 3C and online

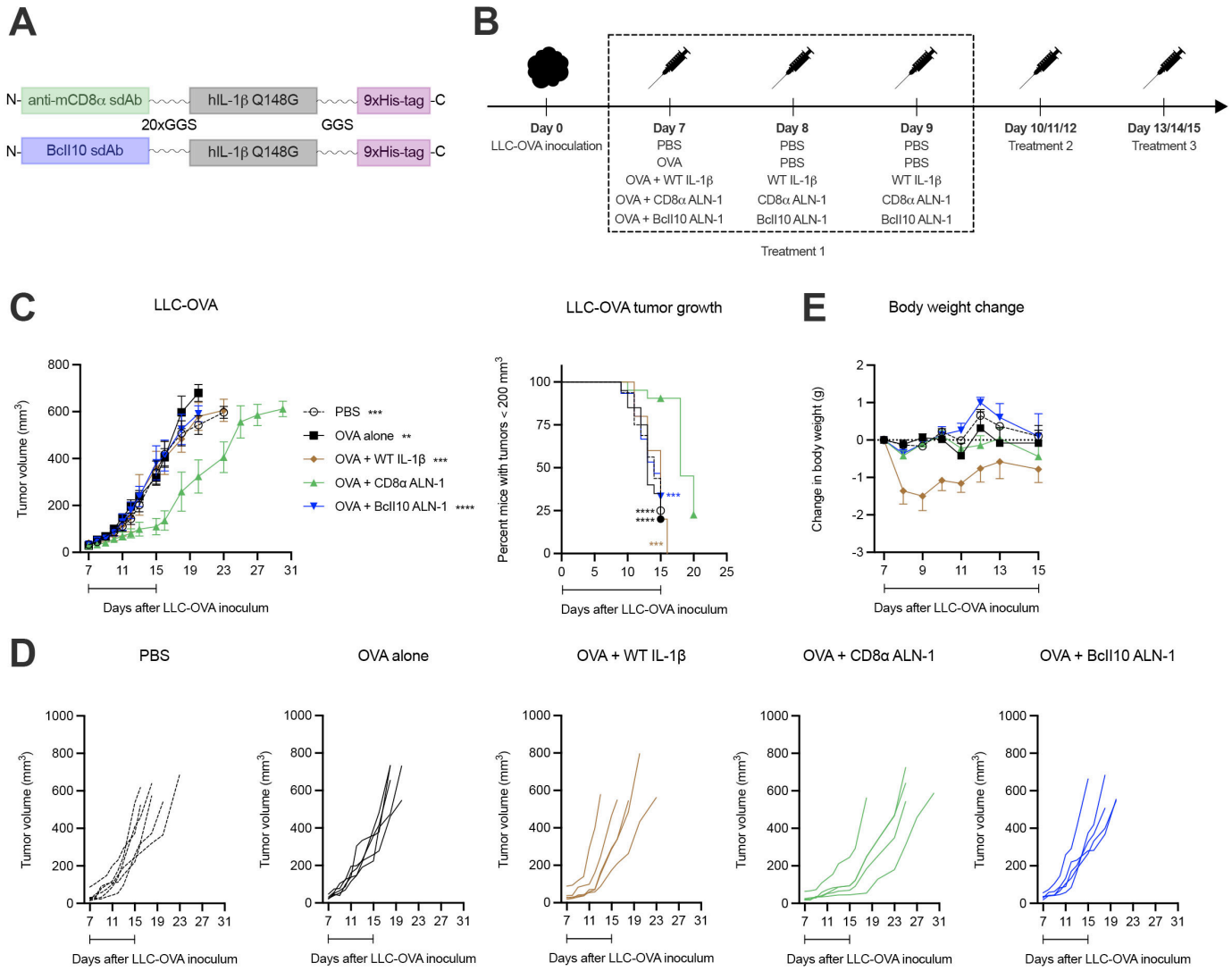

Figure 1 A therapeutic cancer vaccine supplemented with CD8α ALN-1 slows down tumor growth without evoking systemic toxicity. (A) Molecular design of IL-1β AcTakine and BclI10 control. (B) Mice were inoculated with LLC-OVA and treated with OVA (100 µg) or not (PBS). This was combined with treatments with PBS, WT IL-1β (5 µg), CD8α ALN-1 (10 µg) or untargeted BclI10 ALN-1 (10 µg). (C) LLC-OVA tumor growth over time for different treatment conditions (left). Data points represent the mean ± SEM of a representative out of four independent experiments with *n*=6 (PBS) or *n*=5 mice/group. Kaplan-Meier curves demonstrating the required time to reach tumor volumes exceeding 200 mm^3 (right). Data points represent the mean of pooled data from four independent experiments. (D) LLC-OVA tumor growth for individual treatment conditions. Shown is a representative out of four independent experiments. (E) Change in body weight for different treatment conditions. Data points represent the mean ± SEM of a representative out of four independent experiments with *n*=6 (PBS) or *n*=5 mice/group. Intervals below the curves indicate the treatment period. ***p*<0.01, ****p*<0.001, *****p*<0.0001; by two-way ANOVA with Sidak's multiple comparisons test (C) (left) or by log-rank (Mantel-Cox) testing (C) (right). ANOVA, analysis of variance; IL-1β, interleukin-1β; LLC, Lewis lung carcinoma; OVA, ovalbumin; WT, wild-type.

supplemental figure 5A). This robust expansion occurred in all mice and indicates epitope spreading, further evidenced by the top-10 clones covering ≥30% of the top-100. This effect was absent in control mice, where either no clonal expansion or strong dominance of one established clone could be observed. After treatment with CD8α ALN-1, the top-10 most abundant TCRB sequences in TDLN also appeared more diverse in terms of V/J pairing usage (figure 3D). Regarding the top-100 TDLN clones, average V/J pairing usage frequencies revealed spread of the CTL response over numerous smaller TCRB V/J pairs in mice treated with CD8α ALN-1, whereas T cells isolated from controls were enriched in a smaller selection of V/J combinations (figure 3E,F and online supplemental figure 5B). Examination of matched tissues learned that more clones from the TDLN top-100 could be retrieved in tumors upon treatment with OVA + CD8α ALN-1 and several of these clones also expanded (figure 3G). Additionally, average V/J pairing usage frequencies in the tumor show oligoclonal expansion of $CD8^+$ T cells for certain TCRB V/J sequences after treatment with OVA + CD8α ALN-1 (figure 3H and online supplemental figure 5C–F). Collectively, these data present evidence that the

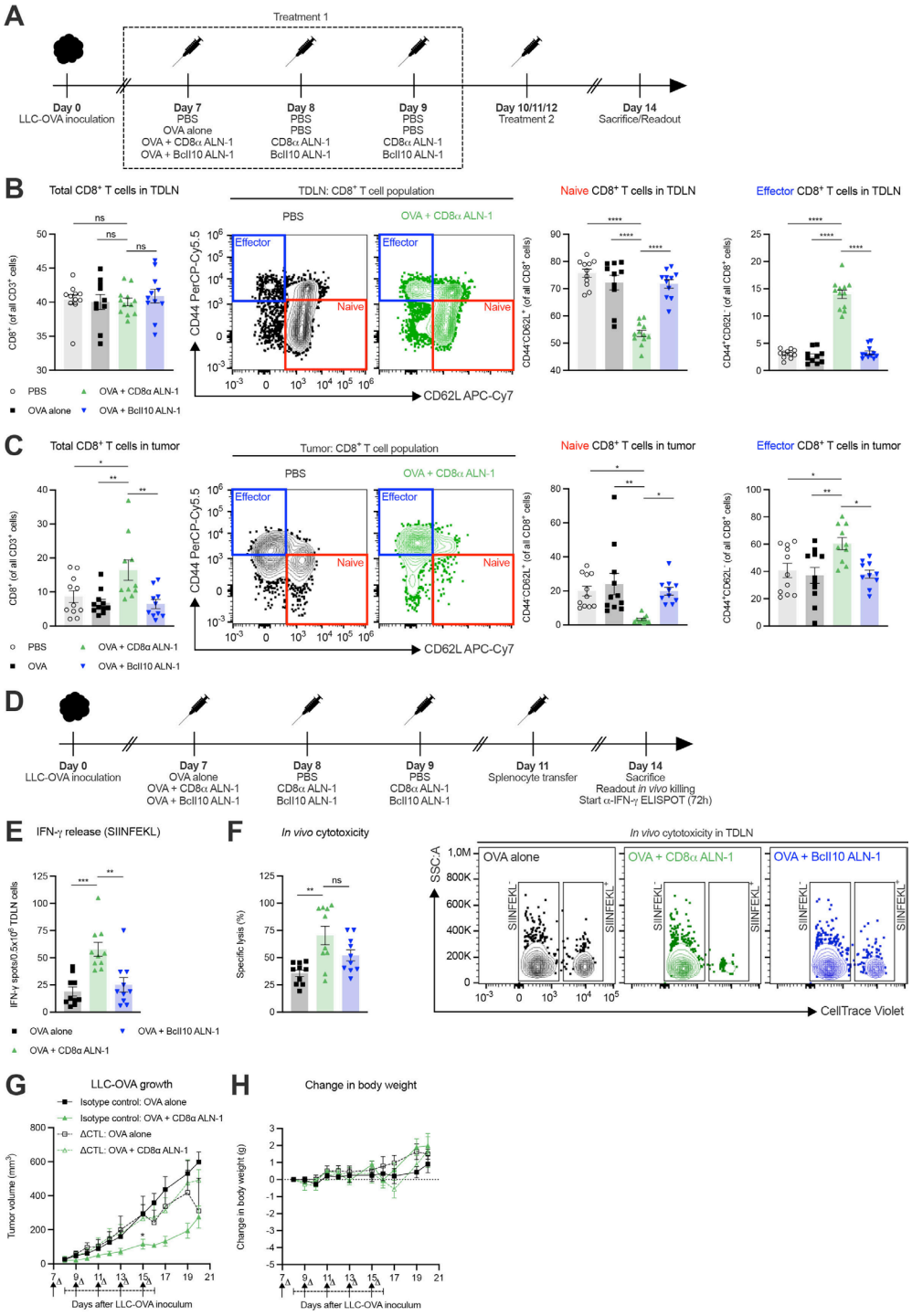

Figure 2 The antitumor effect of CD8α ALN-1 depends on activation of endogenous CD8+ T cell immune responses. (A) Mice inoculated with LLC-OVA received OVA (100 µg) or not (PBS) and were treated with PBS, CD8α ALN-1 (10 µg) or BclI10 ALN-1 (10 µg). (B, C) Frequencies of total, naive and effector CD8+ T cells in TDLN (B) and tumor tissue (C). Bars represent the mean ± SEM of a pool of two independent experiments with *n*=12 mice/group combined with representative flow cytometry dot plots. (D) Mice inoculated with LLC-OVA received OVA alone (100 µg), OVA + CD8α ALN-1 (10 µg) or OVA + BclI10 ALN-1 (10 µg) and splenocyte transfer. (E) IFN-γ release after splenocyte *ex vivo* restimulation, measured by ELISpot. (F) Cytotoxicity toward SIINFEKL+ cells with representative flow cytometry dot plots (right). Bars represent the mean ± SEM of a pool of two independent experiments with *n*=10 mice/group combined. (G) Growth of LLC-OVA in mice treated with a CTL-depleting monoclonal antibody (250 µg) or an isotype control (250 µg). (H) Change in body weight of the mice shown in (G). Antibody administration is indicated by arrows, the treatment period is designated by an interval. Data points represent the mean ± SEM of an experiment with *n*=5 mice/group. **p*<0.05, ***p*<0.01, ****p*<0.001, *****p*<0.0001; ns, *p*≥0.05 by one-way ANOVA with Tukey's multiple comparisons test in (B, C, E, F) or by two-way ANOVA with Sidak's multiple comparisons test in (G). See also online supplemental figures 1 and 2). ANOVA, analysis of variance; IFN-γ, interferon-γ; LLC, Lewis lung carcinoma; ns, not significant; OVA, ovalbumin; TDLN, tumor-draining lymph node.

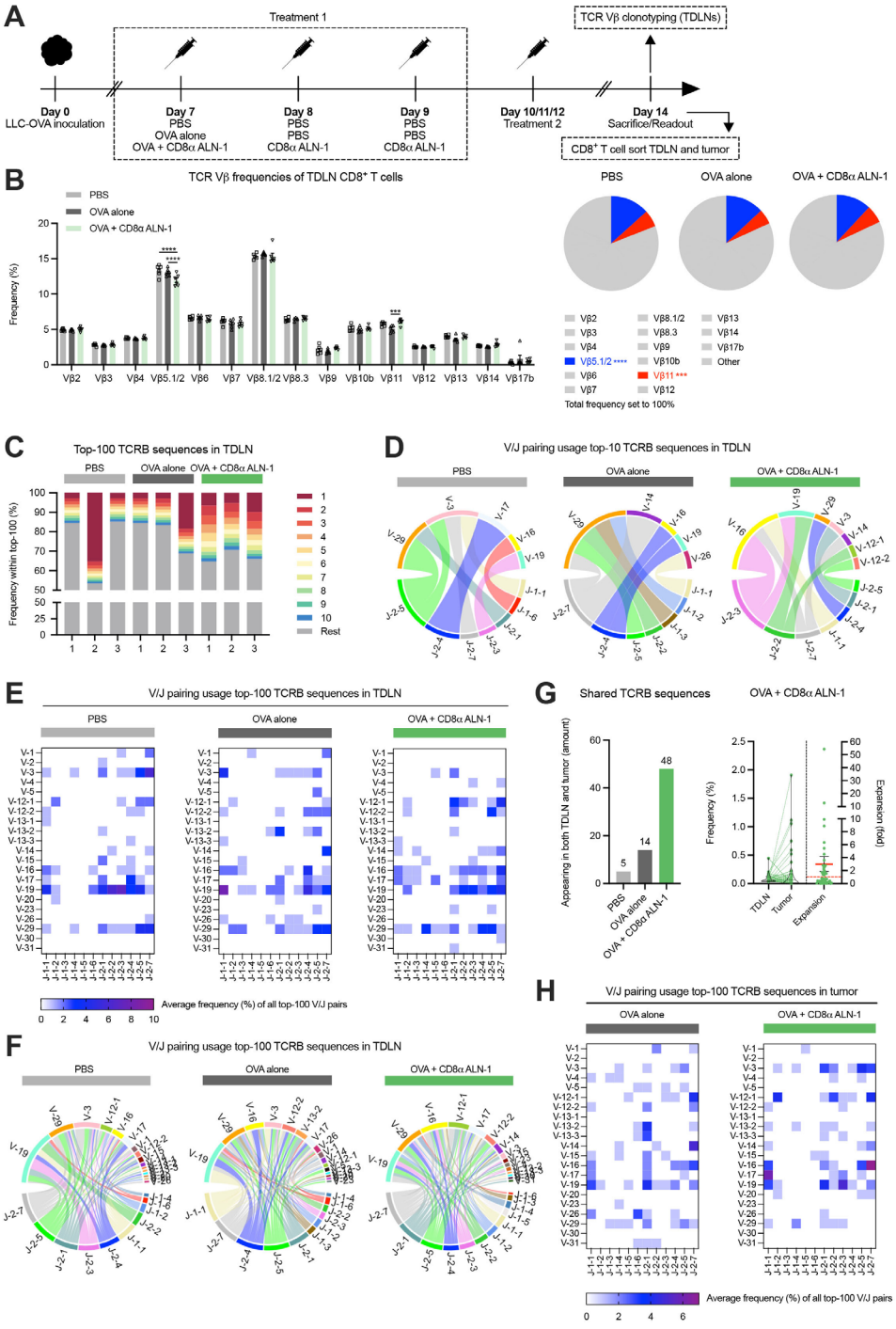

Figure 3 TCR repertoire analysis reveals increased host CTL diversity induced by CD8α ALN-1. (A) Mice inoculated with LLC-OVA received treatment with OVA (100 µg) or not (PBS) in combination with PBS or CD8α ALN-1 (10 µg). (B) Frequencies of 15 different TCR Vβ clonotypes within the CD8$^+$ T cell population (left) with parts-of-whole (right) representing cumulative frequencies of analyzed clonotypes. Remaining unannotated clonotypes are indicated as 'other', colored fractions indicate clonotypes for which statistically significant changes were observed. Bars represent the mean ± SEM of an experiment with n=6 mice/group. ***p<0.001, ****p<0.0001 by two-way ANOVA with Sidak's multiple comparisons test. (C) Frequency of the top-10 most abundant TCRB sequences (stacked bars in color) within the top-100 most abundant TDLN TCRB sequences. The same color does not necessarily represent the same clonotype in the different bars. (D–F) V/J pairing usage within the top-10 (D) and the top-100 (E) and (F) most abundant TDLN TCRB sequences. (G) Amount of sequences from the top-100 TDLN TCRB sequences that are retrieved in matched tumors (left). Relative frequencies of shared sequences in the TDLN and tumor from mice treated with OVA + CD8α ALN-1. Relative expansion of shared sequences in the tumor with the mean relative expansion (red full line) ± SEM; red dotted line indicates relative expansion of 1 (right). (H) V/J pairing usage within the top-100 most abundant TCRB sequences in the tumor. See also online supplemental figures 3–5 and table 2. ANOVA, analysis of variance; CTL, cytotoxic T lymphocytes; LLC, Lewis lung carcinoma; OVA, ovalbumin; TCR, T cell receptor; TDLN, tumor-draining lymph node.

antitumor response mediated by CD8α ALN-1 correlates with clonal expansion (online supplemental figure 5G and H) and increased TCR repertoire diversity in the TDLN and the tumor tissue, implying epitope spreading.

Treatment with CD8α ALN-1 empowers activation and proliferation of adoptively transferred tumor-specific CD8⁺ T cells

Next, we examined whether CD8α ALN-1 empowers activation and proliferation of adoptively transferred OVA-specific CD8⁺ T cells in response to TAA encounter (figure 4A). In mice with established B16- or LLC-OVA tumors, CD8α ALN-1 strongly promoted OT-I CD8⁺ T cell accumulation, proliferation and activation, measured as enhanced PD-1 surface expression, in the TDLN compared with control mice (figure 4B–E, see online supplemental figure 6 for the gating strategy). Of note, more pronounced effects were consistently observed in LLC-OVA⁺ mice. The proliferation index, defined as the fraction of OT-I CD8⁺ T cells in a certain stage of cell division, shows that treatment with CD8α ALN-1 not only engaged more OT-I CD8⁺ T cells to initiate proliferation, but these cells also completed more divisions (figure 4F). This is especially apparent in LLC-OVA⁺ mice, where treatment with CD8α ALN-1 pushed proliferation to the latest stages. We could measure comparable effects in the pmel-model, where CD8⁺ T cells with reactivity toward the gp100 antigen are transferred in mice that carry B16 gp100⁺ melanomas (online supplemental figure 7). Together, these data show that CD8α ALN-1 acts as a potent cellular adjuvant that enhances accumulation, proliferation and activation of adoptively transferred tumor-specific CD8⁺ T cells in response to TAA encounter.

CD8α ALN-1 enhances the efficacy of ATCT by endorsing effector CD8⁺ T cell generation in both TDLN and TME

We next examined whether combination of CD8α ALN-1 with OT-I CD8⁺ T cell transfer could improve the therapeutic window of ATCT. Control mice did not receive ATCT and were treated with OVA, either alone or combined with CD8α ALN-1 (figure 5A). Only three CD8α ALN-1 administrations strongly empowered the therapeutic efficiency of ATCT (figure 5B). Compared with mice that received ATCT alone, the combination with CD8α ALN-1 significantly increased the relative amount of OT-I CD8⁺ T cells and the fraction of effector OT-I CD8⁺ T cells in the TDLN (figure 5C, see online supplemental figure 8A for the gating strategy). As expected, this corresponded with an increase in T-bet expression in both the total and the effector OT-I CD8⁺ T cell population in the TDLN of CD8α ALN-1-treated mice compared with controls.

Also in tumors, combination of ATCT with CD8α ALN-1 yielded larger amounts of effector OT-I CD8⁺ T cells and enhanced T-bet expression in both the total and the effector OT-I CD8⁺ T cell population (figure 5D). After *ex vivo* splenocyte restimulation, we observed more release of IFN-γ and TNF by OT-I CD8⁺ T cells from mice that received ATCT in combination with CD8α ALN-1 (figure 5E). Comparable effects were observed when the total population of CD8⁺ T cells in the TDLN, tumor tissue and spleen of LLC-OVA⁺ mice was considered (online supplemental figure 9A–C, see online supplemental figure 8B) for the gating strategy). In the tumor, treatment with CD8α ALN-1 reduced the relative amount of CD8⁺ T cells with a dysfunctional profile, characterized by expression of CD101 and CD38, and enhanced expression of the transcription factor TCF-1 (online supplemental figure 9D).[28] These latter results are of particular interest in light of recent findings that have linked stem cell-like properties to TCF-1⁺ CD8⁺ T cells and correlated those with a positive clinical response to checkpoint inhibition.[29 30] In conclusion, CD8α ALN-1 empowers ATCT efficiency by enhancing accumulation of functionally potent effector CD8⁺ T cells in the TDLN and the tumor.

cDC1s are dispensable for the cellular adjuvant effect of CD8α ALN-1, but lower the threshold for efficient CD8⁺ T cell proliferation

As murine cDC1s are CD8α⁺ and can thus be a target for CD8α ALN-1, we looked into their activation status in the TDLN (figure 6A). While the relative amount of cDC1s within the total cDC population remained unaltered, we measured a significant increase in cDC2 percentages following treatment with OVA + CD8α ALN-1 compared with PBS and OVA alone (figure 6B, see online supplemental figure 10 for the gating strategy). cDC1s and cDC2s both upregulated the activation markers CD40 and CD86 following treatment with OVA + CD8α ALN-1 (figure 6C,D). Of note, no significant difference in CD86 expression on cDC1s and CD40/CD86 expression on cDC2s was found between treatment with OVA + CD8α ALN-1 and OVA + untargeted BcII10 ALN-1.

Because cDC1s are critical for activation of CD8⁺ T cells, we evaluated their necessity for the adjuvant effect of CD8α ALN-1 (see online supplemental figure 11 for the gating strategy). Both in WT and full-body Batf3$^{-/-}$ mice, treatment with OVA + CD8α ALN-1 significantly increased the frequency of effector CD8⁺ T cells in the TDLN and their expression of T-bet and Eomes (online supplemental figure 12A nd B). Absence of cDC1s reduced T-bet expression in CD8⁺ T cells (online supplemental figure 12B) and increased the fraction of Eomes⁺T-bet^{dim} effector CD8⁺ T cells induced upon CD8α ALN-1 delivery (online supplemental figure 12C). Additionally, we transferred OT-I CD8⁺ T cells in WT or full-body Batf3$^{-/-}$ mice and measured proliferation in the TDLN (figure 6E, see online supplemental figure 13A for the gating strategy). In Batf3$^{-/-}$ mice, fewer OT-I CD8⁺ T cells were present in the TDLN (online supplemental figure 13B), yet treatment with CD8α ALN-1 still promoted their proliferation (figure 6F). While treatment with OVA + CD8α ALN-1 does activate cDCs in the TDLN, presence of cDC1s does not seem to be fundamental for its adjuvant effect. However, signals rendered by cDC1s facilitate the CD8⁺ T cell response following treatment with CD8α ALN-1, for instance by lowering the threshold for expansion.

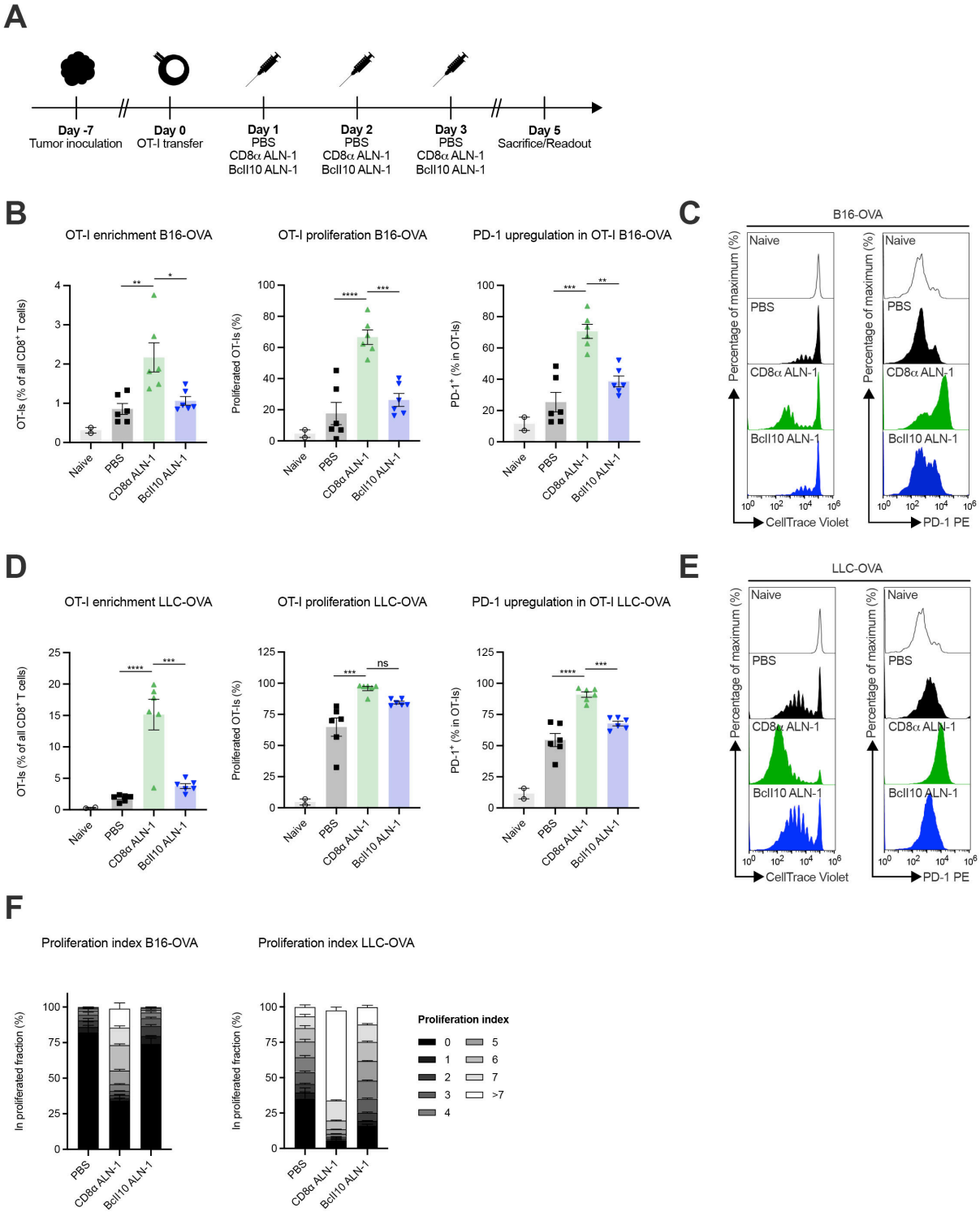

Figure 4 Treatment with CD8α ALN-1 empowers activation and proliferation of adoptively transferred tumor-specific CD8+ T cells. (A) Mice inoculated with B16- or LLC-OVA received OT-I CD8+ T cells and treatments with PBS, CD8α ALN-1 (10 µg) or BclI10 ALN-1 (10 µg). (B–E) Frequencies of OT-I CD8+ T cells within the total CD8+ T cell population in TDLN (left), percentage of total proliferated OT-I CD8+ T cells (middle) and expression of PD-1 on OT-I CD8+ T cells (right) in B16- (B) and LLC-OVA (D) tumor-bearing mice. Bars represent the mean ± SEM of a representative of two independent experiments with *n*=2 (naive) or *n*=6 mice/group. Representative flow cytometry histograms displaying OT-I CD8+ T cell proliferation (left) and PD-1 upregulation (right) in TDLN of B16- (C) and LLC-OVA (E) tumor-bearing mice. (F) Stacked histograms summarize the proliferation index of OT-I CD8+ T cells in B16- (left) and LLC-OVA (right) tumor-bearing mice. Individual stacks represent the mean percentages of proliferating OT-I CD8+ T cells in certain stages of cell division ±SEM. Shown is a representative of two independent experiments with *n*=6 mice/group. **p*<0.05, ***p*<0.01, ****p*<0.001, *****p*<0.0001; ns, p≥0.05 by one-way ANOVA with Tukey's multiple comparisons test. See also online supplemental figures 6 and 7. ANOVA, analysis of variance; LLC, Lewis lung carcinoma; ns, not significant; OVA, ovalbumin; TDLN, tumor-draining lymph node.

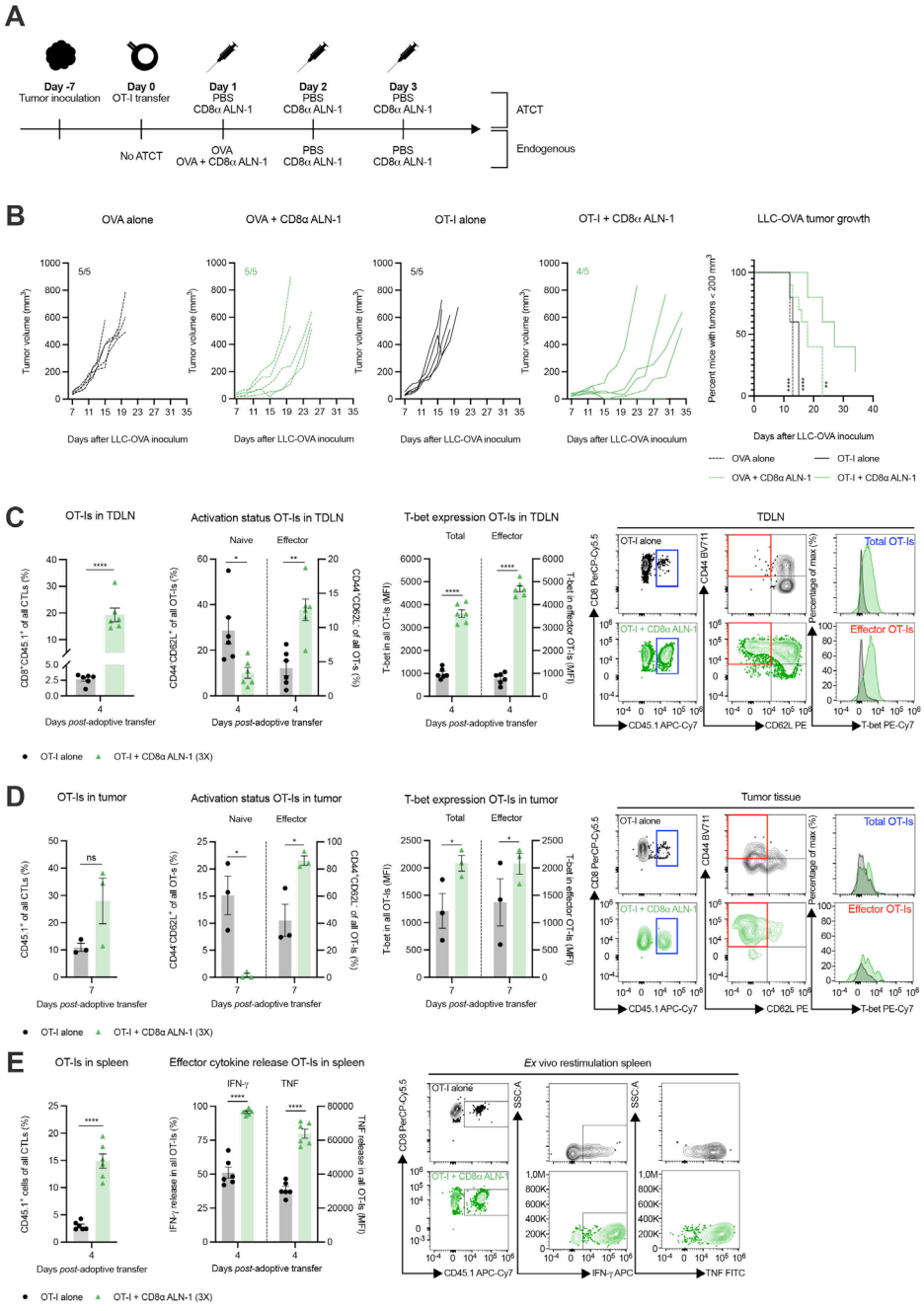

Figure 5 CD8α ALN-1 enhances the efficacy of adoptive T cell transfer by endorsing effector CD8$^+$ T cell generation in both tumor-draining lymph node and tumor microenvironment. (A) Mice carrying established LLC-OVA tumors received OT-I CD8$^+$ T cells and treatment with PBS or CD8α ALN-1 (10 µg). Controls did not receive OT-I CD8$^+$ T cells and were treated with OVA alone (100 µg) or combined with CD8α ALN-1 (10 µg). (B) LLC-OVA tumor growth. Lines represent individual mice. Shown is a representative of two independent experiments with *n*=5 mice/group. Kaplan-Meier curves demonstrate time to reach tumor volumes exceeding 200 mm^3. Pooled data from two independent experiments with *n*=10 mice/group combined. (C, D) Frequencies of OT-I CD8$^+$ T cells within total CD8$^+$ T cells, naive and effector phenotypes within OT-I CD8$^+$ T cells and T-bet expression within the total and effector OT-I CD8$^+$ T cell population in the TDLN (C) and tumor tissue (D) with representative flow cytometry dot plots. (E) Frequencies of OT-I CD8$^+$ T cells within the total CD8$^+$ T cell population and production of IFN-γ and TNF by OT-I CD8$^+$ T cells following *ex vivo* splenocyte restimulation with representative flow cytometry dot plots. Bars represent the mean ± SEM of an experiment with *n*=6 mice/group (for TDLN and spleen samples) or *n*=3 mice/group (for tumor samples, as two mice were pooled together). *p<0.05, **p<0.01, ****p<0.0001; ns, p≥0.05 by log-rank (Mantel-Cox) testing (B) or by unpaired Student's t-test (C–E). See also online supplemental figure 8 and 9. IFN-γ, interferon-γ; LLC, Lewis lung carcinoma; ns, not significant; OVA, ovalbumin; TDLN, tumor-draining lymph node; TNF, tumor necrosis factor.

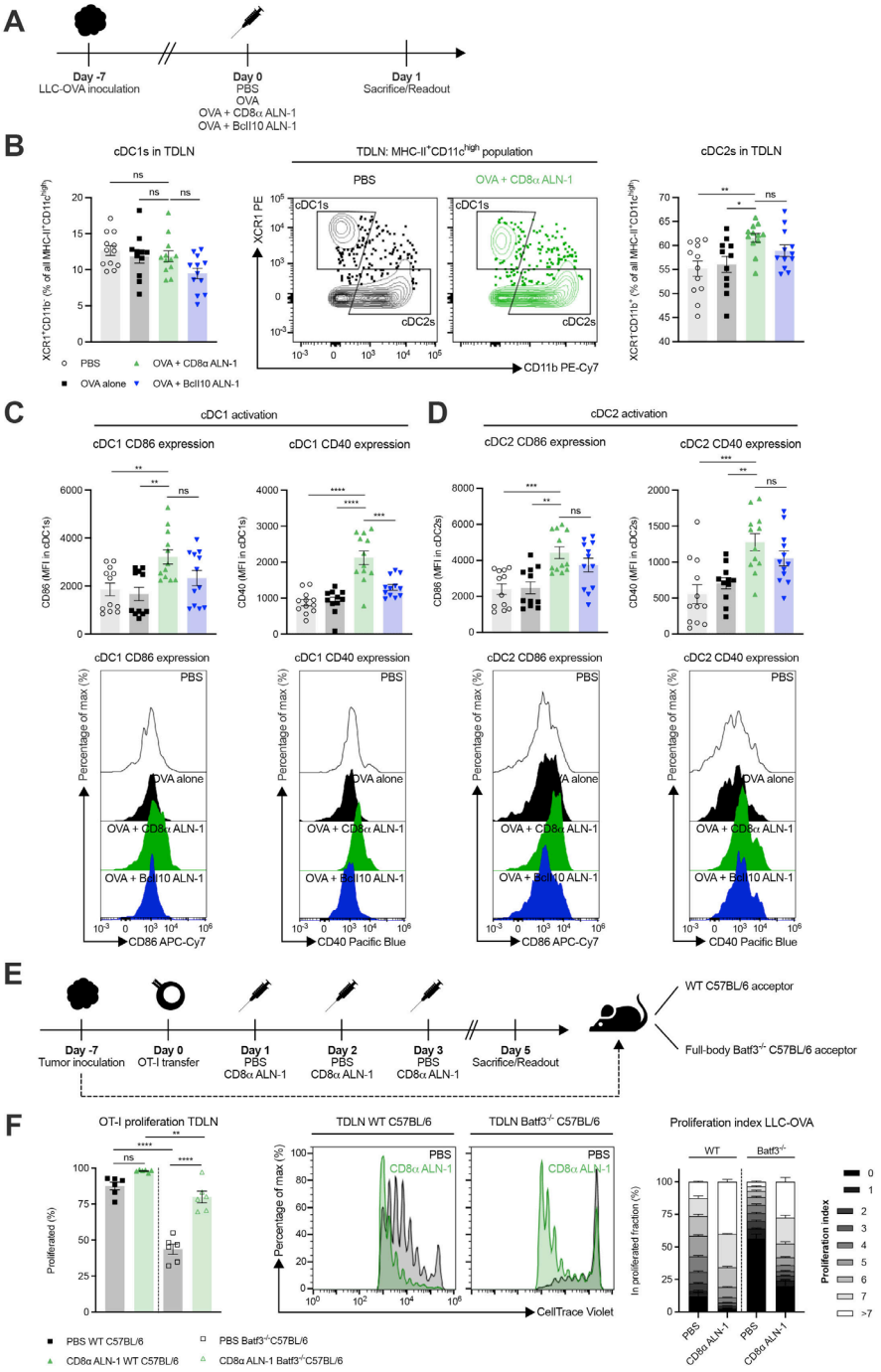

Figure 6 cDC1s are dispensable for the cellular adjuvant effect of CD8α ALN-1, but lower the threshold for efficient CD8$^+$ T cell proliferation. (A) Mice with established LLC-OVA tumors were treated with either PBS, OVA alone (100 µg) or combined with CD8α ALN-1 (10 µg) or untargeted BclI10 ALN-1 (10 µg). (B) Relative amounts of cDC1s (left) and cDC2s (right) within the total cDC population with representative flow cytometry dot plots (middle). (C, D) Expression of the activation markers CD40 (left) and CD86 (right) on cDC1s (C) and cDC2s (D) with representative flow cytometry histograms (bottom). (E) OT-I CD8$^+$ T cells were adoptively transferred in WT or full-body Batf3$^{-/-}$ C57BL/6 mice carrying established LLC-OVA tumors. Acceptor mice received treatments with either PBS or CD8α ALN-1 (10 µg). (F) Fraction of proliferated OT-I CD8$^+$ T cells (left) with representative flow cytometry histograms (middle). Stacked histograms summarize the proliferation index of OT-I CD8$^+$ T cells in WT or full-body Batf3$^{-/-}$ tumor-bearing acceptor mice (right). Bars represent the mean ± SEM of a pool of two independent experiments with n=12 mice/group combined (B–D) or an experiment with n=6 mice/group (F). *p<0.05, **p<0.01, ***p<0.001, ****p<0.0001; ns, p≥0.05 by one-way ANOVA with Tukey's multiple comparisons test. See also online supplemental figures 10–13. ANOVA, analysis of variance; LLC, Lewis lung carcinoma; ns, not significant; OVA, ovalbumin; TDLN, tumor-draining lymph node; WT, wild-type.

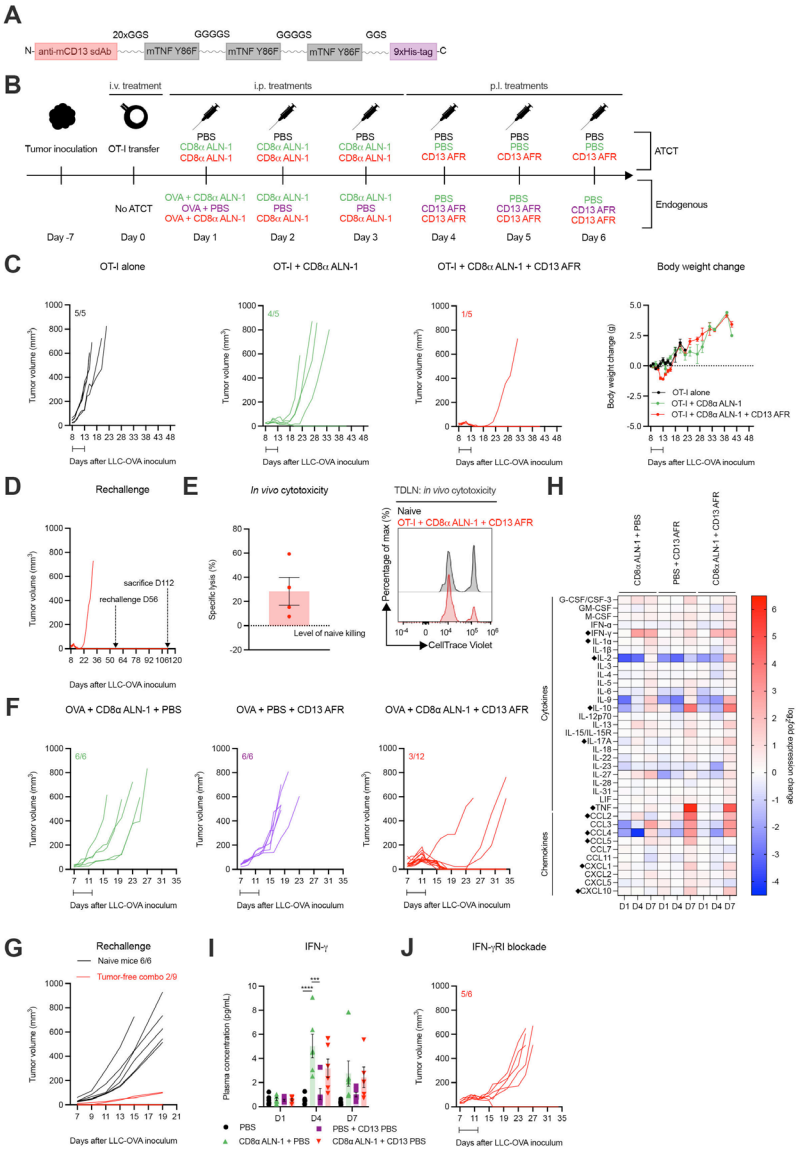

Figure 7 Strong synergy between CD8α ALN-1 and neovasculature-targeted TNF mediates complete tumor eradication in the absence of systemic toxicity and allows for immunological protection against secondary tumor challenge. (A) Molecular TNF AcTakine design. (B) Mice with LLC-OVA tumors received OT-I CD8$^+$ T cell transfer (top) or not (bottom) and were treated with PBS or CD8α ALN-1 (10 µg) in combination with PBS or CD13 AFR (50 µg) (top). Mice not treated with ATCT (bottom) received OVA (100 µg) combined with treatments described above (top). (C) LLC-OVA tumor growth (left) and change in body weight (right) (ATCT). Lines represent individual mice. Data points represent the mean ± SEM of an experiment with *n*=5 mice/group. (D) LLC-OVA tumor growth (ATCT, rechallenge). (E) Cytotoxicity towards SIINFEKL$^+$ cells. Bar represents the mean ± SEM of an experiment with *n*=4 mice/group (left) with representative flow cytometry histograms (right). (F) LLC-OVA tumor growth (without ATCT). Lines represent individual mice of an experiment with *n*=6 or 12 mice/group. (G) LLC-OVA tumor growth (without ATCT, rechallenge). (H) Heat map of $\log_2$-fold changes in plasma cytokine and chemokine levels. Group means of an experiment with *n*=6 mice/group. Statistically significant differences are indicated with a diamond icon. (I) Plasma IFN-γ concentration. Bars represent the mean ± SEM of an experiment with *n*=6 mice/group. ***p<0.001, ****p<0.0001; ns, p≥0.05 by one-way ANOVA with Tukey's multiple comparisons test. (J) LLC-OVA tumor growth. Mice were treated with an anti-mouse IFN-γRI antibody (500 µg) every 48 hours starting 1 day before the first CD8α ALN-1 delivery. Intervals indicate the treatment periods. See also online supplemental figures 14–16. AcTakine, Activity-on-Target cytokine; ANOVA, analysis of variance; ATCT, adoptive T cell transfer; IFN-γ, interferon-γ; IL, interleukin; LLC, Lewis lung carcinoma; ns, not significant; OVA, ovalbumin; TNF, tumor necrosis factor.

Strong synergy between CD8α ALN-1 and neovasculature-targeted TNF mediates complete tumor eradication and protective memory against secondary tumor challenge

Recently, we developed an AcTakine that targets TNF activity (AcTafactor/AFR) to tumor neovasculature via an anti-mouse CD13 sdAb (figure 7A).[31] In this way, the ability of TNF to activate tumor endothelial cells and consequentially promote CTL influx into the tumor can be exploited in the absence of toxicities and undesired off-target side effects. Of note, AFR incorporates

a murine cytokine mutant, as TNF activity, in sharp contrast with that of IL-1β, is highly species-specific. Treatment with CD13 AFR efficiently eradicated large established tumors in different combinations, including ATCT of human CD70 CAR-T cells, without eliciting the toxicities observed with WT TNF. We were, therefore, driven to examine whether combination with CD13 AFR delivery could improve the efficacy of CD8α ALN-1 treatment.

First, we tried to further improve the efficacy of OT-I CD8$^+$ T cell adoptive transfer combined with CD8α ALN-1 treatment by additional delivery of CD13 AFR (figure 7B, upper part). Addition of CD13 AFR allowed for complete eradication of established LLC-OVA tumors with limited loss in body weight (approximately 5%) (figure 7C). Characteristic for this antitumor effect is strong and complete tumor necrosis, allowing mice to remain tumor-free for >50 days after inoculation. Importantly, these mice were fully protected against secondary tumor challenge, which correlated with CD8$^+$ T cell-mediated cytotoxicity (figure 7D,E). We next combined treatment with OVA + CD8α ALN-1 with CD13 AFR administration, without prior ATCT (figure 7B, bottom part). In this completely endogenous model, the combination induced full tumor eradication in 9/12 mice (figure 7F). Whereas naive mice could not control tumor growth after rechallenge, 7/9 mice previously treated with CD8α ALN-1 and CD13 AFR were protected (figure 7G). Comparable results could be obtained in the B16 melanoma model (online supplemental figure 14).

In order to mechanistically understand this AcTakine synergy, we sampled blood from LLC-OVA$^+$ mice and analyzed cytokine and chemokine plasma levels using a Luminex multiplex assay (online supplemental figure 15A). Treatment with CD8α ALN-1 significantly enhanced IFN-γ levels compared with PBS treatment (figure 7H,I). IFN-γ has been described to enhance sensitivity of tumor endothelial cells for TNF activity and could therefore be an important mediator of this synergy.[31] Indeed, on systemic administration of an anti-mouse IFN-γRI antibody in LLC-OVA$^+$ mice, treatment with CD8α ALN-1 combined with CD13 AFR only induced complete tumor necrosis in one in five mice (figure 7J). Multiplex analysis further revealed that only CD13 AFR increases plasma levels of different chemokines, including CCL2, CCL4, CCL5, CXCL1 and CXCL10, and IL-10 (figure 7H and online supplemental figures 15B and 16). Combination of CD8α ALN-1 and CD13 AFR enhanced IL-2 and IL-17A release compared with PBS treatment or monotherapy. In summary, CD8α ALN-1 promotes proliferation and effector functionality of antitumor CD8$^+$ T cells and synergizes with CD13 AFR to mediate complete tumor eradication, allowing protection against secondary challenge. This AcTakine combination is empowered by IFN-γ, which is probably released by CD8α ALN-1-activated CD8$^+$ T cells and sensitizes the TME for TNF.

DISCUSSION

The current mantra in the search for stronger and more durable antitumor T cell responses can be summarized as 'releasing the breaks, pushing the gas pedal'. The former can be achieved by inhibition of immune checkpoints, which represent molecules that keep the immune response 'in check' following its initiation. Considerable clinical success has been booked by interfering with the interaction between PD-1 and its ligands. 'Pushing the gas', on the other hand, has not yet achieved the same extent of results. Personalized cancer vaccines based on tumor-derived neoantigens could be an important leap forward, but their efficacy will depend on potent adjuvants that are able to drive T cell immunity.

To widen the therapeutic window of cytokines with valuable therapeutic properties, we devised AcTakines, which represent a novel class of immunocytokines with the potential to circumvent the toxicities (*e.g.*, severe body weight loss, influenza-like symptoms and cytokine storm) and unwanted side effects associated with systemic administration of WT cytokines and conventional immunocytokines. Here, we report the use of an IL-1β-based AcTakine as a cellular adjuvant to promote antitumor T cell responses. We previously demonstrated that this AcTakine acts as a potent and safe adjuvant in influenza vaccination by stimulating CD8$^+$ T cell effector function and memory differentiation.[26] Considering the high need for powerful drivers of antitumor immunity, we explored the adjuvant effect of this AcTakine in cancer immunotherapy.

As a monotherapy, CD8α ALN-1 showed a modest effect on tumor growth, which was absent in mice that received WT IL-1β or untargeted BcII10 ALN-1. This demonstrates the advantage of selective delivery of IL-1 activity to CD8α$^+$ cells, but despite this, the observed antitumor response was incomplete. Indeed, tumor sizes in mice that received CD8α ALN-1 quickly caught up with those in control animals. Nonetheless, treatment with CD8α ALN-1 massively increased CD8$^+$ T cell expansion and shifted the naive/effector-ratio towards the latter in the TDLN and tumor. Moreover, these T cells readily released IFN-γ on *ex vivo* restimulation and exerted potent cytolytic activity *in vivo*, which further endorses their effector phenotype. The importance of CD8$^+$ T cells in this antitumor response was confirmed by the loss of the treatment effect following their depletion. We found that delivery of IL-1 activity to CD8α$^+$ cells outperformed treatment with WT IL-1β, likely due to circumvention of the cytokine's protumorigenic properties.[20] Besides improved antitumor action, we noticed a drastic reduction in toxicity on administration of CD8α ALN-1, which is in accordance with data from our earlier work.[26]

How cancer vaccines will deal with tumor heterogeneity remains an important concern. As tumors are highly polyclonal, the breadth of the CD8$^+$ T cell response will be an important determinant of clinical efficacy.[12] Indeed, clinical studies have demonstrated that patients with the best objective responses to DC vaccination showed evidence

of epitope spreading.[32 33] Earlier work demonstrated that inflammatory cytokines can fine-tune the sensitivity of TCRs, theoretically allowing for a more diverse T cell response in terms of epitope recognition.[34] Whether this applies for IL-1β activity is currently unknown and therefore, we evaluated the TCR repertoire of $CD8^+$ T cells following treatment with CD8α ALN-1. Using a flow cytometry-based method, we noticed a moderate shift in the TCR clonotype use of $CD8^+$ T cells. Although this effect is rather modest, Lai *et al.* observed a comparable response within the tumor-specific OT-I $CD8^+$ T cell subset,[27] while we assessed the endogenous bulk $CD8^+$ T cell population. Using TCR sequencing, we found that CD8α ALN-1 empowers epitope spreading in the TDLN by increasing the frequency of multiple unique T cell clones in the TDLN. In accordance with our flow cytometry data, CD8α ALN-1 facilitated trafficking of different T cell clones from the TDLN to the TME and enables their oligoclonal expansion at the tumor site. While the results from these experiments are convincing, more pronounced epitope spreading could theoretically be expected in absence of OVA, which is a relatively immunogenic model antigen. How IL-1 exactly mediates these effects warrants further research and more insight in this process could be extremely valuable to improve effectivity of adjuvants focused at driving cellular immunity. A potential mechanism could be lowering of the antigen sensitivity threshold of $CD8^+$ T cells by modulation of downstream TCR signaling, which has been observed for other proinflammatory cytokines, including type I IFN, IL-12 and the IL-1 superfamily member IL-18.[34 35]

Unlike human cDC1s, murine cDC1s express CD8α[36] and represent an additional target for CD8α ALN-1. Indeed, we noticed upregulation of the activation markers CD40 and CD86 on TDLN cDC1s after treatment with CD8α ALN-1, which is in line with earlier reports.[15 37] As can be expected from the critical role of cDC1s in the cancer-immunity cycle,[1] basal proliferation of OT-I $CD8^+$ T cells in response to TAA was strongly reduced in full-body $Batf3^{-/-}$ mice, which lack a functional cDC1 compartment. While less T cells engaged in cell division, CD8α ALN-1 could still empower $CD8^+$ T cells that initiated proliferation, independent of cDC1s. Effector differentiation of endogenous $CD8^+$ T cells by CD8α ALN-1 was not influenced in absence of cDC1s, yet we did observe differences in T-bet and Eomes expression. $Eomes^+T\text{-}bet^{dim}$ $CD8^+$ T cells were increased in $Batf3^{-/-}$ mice after CD8α ALN-1 treatment, a phenotype described by Jia *et al.* to be functionally impaired and correlated with poor prognosis in acute myeloid leukemia.[38] However, these results should be cautiously interpreted, as recent studies reported on the importance of T cell-intrinsic Batf3 expression during memory $CD8^+$ T cell and T_H9 $CD4^+$ T cells development.[39 40]

Cancer vaccines are challenged by the vast amount of tumor mass the immune system must face. Vaccine-induced $CD8^+$ T cells need to take on billions of cancer cells in immunosuppressive environments, which contributes to their limited efficacy.[12] Results from clinical studies have shown that cancer vaccines can elicit measurable reactions, but these seldomly evolve into an objective response.[41] We therefore sought to combine OT-I $CD8^+$ T cell infusion with CD8α ALN-1 administration, as some studies have suggested that combination of ATCT and cancer vaccination could be a valuable strategy.[42 43] While delivery of OT-I $CD8^+$ T cells alone had no effect on tumor growth, additional administration of only three shots of CD8α ALN-1 prolonged tumor control, even causing complete responses in some mice. CD8α ALN-1 strongly shifted the phenotype of the infused T cells towards an effector phenotype, characterized by a $CD44^+CD62L^-$ profile and T-bet expression, in the TDLN and the tumor. These results are in accordance with data shown by Lee *et al.*, who demonstrated comparable effects with WT IL-1β.[18] Of note, more pronounced effects on OT-I $CD8^+$ T cell proliferation after treatment with CD8α ALN-1 could be observed in LLC-OVA compared with B16-OVA, which can potentially be explained by differences in OVA presentation, composition of the TME[44] and lesion sizes at the time of T cell infusion. Revitalization of endogenous T cells could be essential for achieving optimal therapeutic efficiency of ATCT.[45] Combination of OT-I $CD8^+$ T cell transfer with CD8α ALN-1 treatment not only activated the transferred T cells, but also elicited comparable effects within the endogenous $CD8^+$ T cell population. We measured a decrease in terminally dysfunctional ($CD101^+/CD38^+$) and an increase in stem cell-like ($TCF\text{-}1^+$) endogenous $CD8^+$ T cells in tumors of mice that received CD8α ALN-1, which has previously been described to be essential for durable antitumor responses to immunotherapy.[46 47] The observed upregulation of PD-1 on OT-I $CD8^+$ T cells following their activation by CD8α ALN-1 also provides a rationale to investigate whether additional combination treatment with anti-PD-1 or anti-PD-L1 monoclonal antibodies could further enhance therapeutic efficacy.

We went on to study the therapeutic effect of the combination between CD8α ALN-1 and CD13 AFR, which represents an AcTakine that delivers TNF to tumor endothelial cells by targeting the neovasculature marker aminopeptidase N (CD13).[31 48] The rationale behind this combination is the dual effect that can potentially be achieved: (1) enhanced expansion and effector differentiation of antitumor $CD8^+$ T cells; and (2) improved tumor trafficking as a consequence of tumor neovasculature activation. Earlier work demonstrated that CD13 AFR acts on HUVECs to drive ICAM-1 expression,[31] which mediates TME infiltration of activated $CD8^+$ T cells.[49] Sequential delivery of CD8α ALN-1 and CD13 AFR induced rapid and complete tumor necrosis, characterized by conversion of the tumor mass into a scab that eventually disappeared and completely healed. Mice that received this treatment remained tumor-free for several weeks and

were protected against a secondary challenge, which indicates the presence of immunological memory.

This effect strikingly mirrored the phenotype that results from combined intratumoral delivery of CD13 AFR and a CD13 IFN-γ-based AcTakine, which has been reported in earlier work by our group.[31] The synergy between IFN-γ and TNF has been extensively documented and recent evidence showed that IFN-γ acts on endothelial cells to enhance TNF sensitivity, probably by upregulation of TNF-RI or apoptotic mediators, such as pro-caspase 8.[31 50] We hypothesized that antitumor $CD8^+$ T cells form a local source of IFN-γ upon their activation by CD8α ALN-1. In the TME, IFN-γ can subsequently lower the threshold for TNF activity, enabling full tumor eradication upon CD13 AFR delivery. Tumor clearance and absence of TAAs allow local $CD8^+$ T cells to differentiate into memory cells, which safeguard the host against rechallenge. We measured more IFN-γ release by $CD8^+$ T cells *ex vivo* and an increase in circulating IFN-γ after treatment with CD8α ALN-1. Moreover, IFN-γRI blockade prevented the synergy between CD8α ALN-1 and CD13 AFR.

The cytokine and chemokine analysis we performed showed that CD13 AFR treatment induces an elevation of IL-10 levels. IL-10 executes anti-inflammatory functions and has been described before to be upregulated by TNF, representing a negative feedback that controls excessive tissue inflammation.[51] CD13 AFR alone also mediates expression of CCR and CXCR family chemokines, indicating that different innate and adaptive immune cells are being recruited to the TME. How these heterogeneous immune populations exactly influence the synergy between IL-1 and TNF activity in the tumor demands further research. Of note, only the sequential delivery of CD8α ALN-1 and CD13 AFR induced IL-2 and IL-17A release, suggesting the initiation of Treg and T_H17 immunity.

While B16 and LLC are commonly used models in cancer research due to their robustness and fast growth, among other reasons, the simplicity of these models represents an important limitation of our study. In order to narrow the gap between bench and bedside, the clinical potential of CD8α ALN-1 as a therapeutic cancer vaccine adjuvant should therefore be further evaluated in orthotopically growing tumor models and patient-derived xenografts.

CONCLUSION

Delivery of IL-1 activity to $CD8^+$ T cells bypasses toxicities and unwanted side effects, while driving proliferation, activation and effector functionality of antitumor T cells. CD8α ALN-1 improves the efficacy of ATCT and synergizes with neovasculature-targeted TNF for full tumor eradication. The synergy between CD8α ALN-1 and CD13 AFR is mediated by IFN-γ, probably produced upon $CD8^+$ T cell activation. This AcTakine/cytokine triumvirate acts as a powerful 'nuke' that mediates tumor destruction and holds promise for further clinical translation.

Twitter Stéphane Plaisance @steph_Plaisance

Acknowledgements We thank the VIB Nanobody Core (Reza Hassanzadeh Ghassabeh) for sdAb selection; the VIB Flow Core (Gert Van Isterdael and Julie Van Duyse) for assistance with optimization of the cell sorting; the VIB Nucleomics Core (Stefaan Derveaux and Ruth Maes) for their help in organizing the TCR repertoire analysis, performing the bulk TCR sequencing and the data processing; Bart Lambrecht for the OT-I TCR transgenic CD45.1 C57BL/6 $Rag2^{-/-}$ C57BL/5 mice; Karine Breckpot for the full-body $Batf3^{-/-}$ C57BL/6 mice and Nicholas P. Restifo for the B16 $gp100^+$ melanoma cell line. The authors wish to thank Ed Lavelle, Kenny Roose, Jo Van Ginderachter, Karim Vermaelen and Andy Wullaert for their very valuable input. BVDE is a doctoral fellow receiving FWO-SB funding (project 1S32118N). This work was supported by an FWO grant (project G045318) awarded to SG and JT and a UGent Methusalem and an Advanced ERC grant (CYRE 340941) awarded to JT. JT heads the Receptor Research Laboratories, which received financial research support for this research from Orionis Biosciences

Contributors NK, GU, SG and JT conceptualized the research and BVDE, LH and SVL helped developing the methodology. BVDE, LH, SVL and EB conducted experiments. BVDE performed statistical analyses. SP performed bioinformatics analysis. FP contributed to CD8α ALN-1 and CD13 AFR design. AC aided in AcTakine and in vivo model optimization. GU was involved in preparing work concerning sdAb selection. BVDE, SG and JT wrote the manuscript. All authors contributed to reviewing and editing of the manuscript. Guarantors: SG and JT.

Funding BVDE is a doctoral fellow receiving FWO-SB funding (project 1S32118N). This work was supported by an FWO grant (project G045318) awarded to SG and JT and a UGent Methusalem and an Advanced ERC grant (CYRE 340941) awarded to JT. JT heads the Receptor Research Laboratories, which received financial research support for this research from Orionis Biosciences.

Competing interests Financial interests: NK and JT are affiliated and hold equity interests in Orionis Biosciences. The following patent applications are related to the work presented in this paper: WO/2015/007542: Targeted modified IL-1 family members. Applicants: VIB VZW, Universiteit Gent, Centre National de la Recherche Scientifique, Université Montpellier, Centre Hospitalier Regional Universitaire de Montpellier. Inventors: JT, SG, FP and GU This patent application describes IL-1β mutants with reduced bioactivity that can be activated by targeting. WO/2017/134306: CD8 binding agents. Applicants: Orionis Biosciences, VIB VZW, Universiteit Gent. Inventors: JT, AC, NK and SG. This patent application describes sdAbs that bind CD8 and that can be used to target mutant IL-1β to CTLs. WO/2015/007903: Targeted modified TNF family members. Applicants: VIB VZW, Universiteit Gent, Centre National de la Recherche Scientifique, Université Montpellier, Centre Hospitalier Regional Universitaire de Montpellier. This patent application describes TNF mutants with reduced bioactivity that can be activated by targeting. Inventors: JT, Jennyfer Bultinck, FP and GU. The authors have no other, nonfinancial, competing interests to declare.

Patient consent for publication Not applicable.

Provenance and peer review Not commissioned; externally peer reviewed.

Data availability statement Data are available in a public, open access repository. All data relevant to the study are included in the article or uploaded as online supplemental information.

ORCID iDs
Bram Van Den Eeckhout http://orcid.org/0000-0002-6729-8951
Leander Huyghe http://orcid.org/0000-0003-1523-7441
Sandra Van Lint http://orcid.org/0000-0001-9767-5386
Stéphane Plaisance http://orcid.org/0000-0002-1651-241X
Frank Peelman http://orcid.org/0000-0001-6852-8731
Anje Cauwels http://orcid.org/0000-0002-5443-7027
Gilles Uzé http://orcid.org/0000-0002-4150-5772
Sarah Gerlo http://orcid.org/0000-0002-1628-6088
Jan Tavernier http://orcid.org/0000-0002-7609-6462

REFERENCES

1 Chen DS, Mellman I. Oncology meets immunology: the Cancer-Immunity cycle. *Immunity* 2013;39:1–10.
2 Alsaab HO, Sau S, Alzhrani R, *et al*. PD-1 and PD-L1 checkpoint signaling inhibition for cancer immunotherapy: mechanism, combinations, and clinical outcome. *Front Pharmacol* 2017;8:1–15.
3 Kim TK, Herbst RS, Chen L. Defining and understanding adaptive resistance in cancer immunotherapy. *Trends Immunol* 2018;39:624–31.
4 Schoenfeld AJ, Hellmann MD. Acquired resistance to immune checkpoint inhibitors. *Cancer Cell* 2020;37:443–55.
5 Fu J, Kanne DB, Leong M, *et al*. Sting agonist formulated cancer vaccines can cure established tumors resistant to PD-1 blockade. *Sci Transl Med* 2015;7:1–11.
6 Ali OA, Lewin SA, Dranoff G, *et al*. Vaccines combined with immune checkpoint antibodies promote cytotoxic T-cell activity and tumor eradication. *Cancer Immunol Res* 2016;4:95–100.
7 Shi LZ, Goswami S, Fu T, *et al*. Blockade of CTLA-4 and PD-1 enhances adoptive T-cell therapy efficacy in an ICOS-Mediated manner. *Cancer Immunol Res* 2019;7:1803–12.
8 Wilgenhof S, Corthals J, Heirman C, *et al*. Phase II study of autologous monocyte-derived mRNA electroporated dendritic cells (TriMixDC-MEL) plus ipilimumab in patients with pretreated advanced melanoma. *JCO* 2016;34:1330–8.
9 McNeel DG, Eickhoff JC, Wargowski E, *et al*. Concurrent, but not sequential, PD-1 blockade with a DNA vaccine elicits anti-tumor responses in patients with metastatic, castration-resistant prostate cancer. *Oncotarget* 2018;9:25586–96.
10 Cao Y, Lu W, Sun R, *et al*. Anti-Cd19 chimeric antigen receptor T cells in combination with nivolumab are safe and effective against relapsed/refractory B-cell non-Hodgkin lymphoma. *Front Oncol* 2019;9:1–11.
11 Wang J, Deng Q, Jiang Y-Y, *et al*. Car-T 19 combined with reduced-dose PD-1 blockade therapy for treatment of refractory follicular lymphoma: a case report. *Oncol Lett* 2019;18:4415–20.
12 Hollingsworth RE, Jansen K. Turning the corner on therapeutic cancer vaccines. *NPJ Vaccines* 2019;4:1–7.
13 Van Den Eeckhout B, Tavernier J, Gerlo S. Interleukin-1 as innate mediator of T cell immunity. *Front Immunol* 2020;11:1–26.
14 Ben-Sasson SZ, Hogg A, Hu-Li J, *et al*. Il-1 enhances expansion, effector function, tissue localization, and memory response of antigen-specific CD8 T cells. *J Exp Med* 2013;210:491–502.
15 Pang IK, Ichinohe T, Iwasaki A. Il-1R signaling in dendritic cells replaces pattern-recognition receptors in promoting $CD8^+$ T cell responses to influenza A virus. *Nat Immunol* 2013;14:246–53.
16 Sarkar S, Yuzefpolskiy Y, Xiao H, *et al*. Programming of CD8 T cell quantity and Polyfunctionality by direct IL-1 signals. *J Immunol* 2018;201:3641–50.
17 Lapuente D, Storcksdieck Genannt Bonsmann M, Maaske A, *et al*. IL-1β as mucosal vaccine adjuvant: the specific induction of tissue-resident memory T cells improves the heterosubtypic immunity against influenza A viruses. *Mucosal Immunol* 2018;11:1265–78.
18 Lee P-H, Yamamoto TN, Gurusamy D, *et al*. Host conditioning with IL-1β improves the antitumor function of adoptively transferred T cells. *J Exp Med* 2019;216:2619–34.
19 Veltri S, Smith JW. Interleukin 1 trials in cancer patients: a review of the toxicity, antitumor and hematopoietic effects. *Stem Cells* 1996;14:164–76.
20 Rébé C, Ghiringhelli F. Interleukin-1β and Cancer. *Cancers* 2020;12:1791–31.
21 Voronov E, Shouval DS, Krelin Y, *et al*. Il-1 is required for tumor invasiveness and angiogenesis. *Proc Natl Acad Sci U S A* 2003;100:2645–50.
22 Krelin Y, Voronov E, Dotan S, *et al*. Interleukin-1beta-driven inflammation promotes the development and invasiveness of chemical carcinogen-induced tumors. *Cancer Res* 2007;67:1062–71.
23 Tu S, Bhagat G, Cui G, *et al*. Overexpression of interleukin-1beta induces gastric inflammation and cancer and mobilizes myeloid-derived suppressor cells in mice. *Cancer Cell* 2008;14:408–19.
24 Kiss M, Vande Walle L, Saavedra PHV, *et al*. IL1β Promotes Immune Suppression in the Tumor Microenvironment Independent of the Inflammasome and Gasdermin D. *Cancer Immunol Res* 2021;9:309–23.
25 Garcin G, Paul F, Staufenbiel M, *et al*. High efficiency cell-specific targeting of cytokine activity. *Nat Commun* 2014;5:1–9.
26 Van Den Eeckhout B, Van Hoecke L, Burg E, *et al*. Specific targeting of IL-1β activity to CD8+ T cells allows for safe use as a vaccine adjuvant. *npj Vaccines* 2020;5:1–17.
27 Lai J, Mardiana S, House IG, *et al*. Adoptive cellular therapy with T cells expressing the dendritic cell growth factor Flt3L drives epitope spreading and antitumor immunity. *Nat Immunol* 2020;21:914–26.
28 Philip M, Fairchild L, Sun L, *et al*. Chromatin states define tumour-specific T cell dysfunction and reprogramming. *Nature* 2017;545:452–6.
29 Sade-Feldman M, Yizhak K, Bjorgaard SL, *et al*. Defining T cell states associated with response to checkpoint immunotherapy in melanoma. *Cell* 2018;175:998–1013.
30 Siddiqui I, Schaeuble K, Chennupati V, *et al*. Intratumoral $Tcf1^+PD\text{-}1^+CD8^+$ T Cells with Stem-like Properties Promote Tumor Control in Response to Vaccination and Checkpoint Blockade Immunotherapy. *Immunity* 2019;50:195–211.
31 Huyghe L, Van Parys A, Cauwels A, *et al*. Safe eradication of large established tumors using neovasculature-targeted tumor necrosis factor-based therapies. *EMBO Mol Med* 2020;12:1–15.
32 Ribas A, Glaspy JA, Lee Y, *et al*. Role of dendritic cell phenotype, determinant spreading, and negative costimulatory blockade in dendritic cell-based melanoma immunotherapy. *J Immunother* 2004;27:354–67.
33 Butterfield LH, Comin-Anduix B, Vujanovic L, *et al*. Adenovirus MART-1–engineered autologous dendritic cell vaccine for metastatic melanoma. *J Immunother* 2008;31:294–309.
34 Richer MJ, Nolz JC, Harty JT. Pathogen-specific inflammatory milieux tune the antigen sensitivity of CD8+ T cells by enhancing T cell receptor signaling. *Immunity* 2013;38:140–52.
35 Raué H-P, Beadling C, Haun J, *et al*. Cytokine-mediated programmed proliferation of virus-specific CD8(+) memory T cells. *Immunity* 2013;38:131–9.
36 Vremec D, Zorbas M, Scollay R, *et al*. The surface phenotype of dendritic cells purified from mouse thymus and spleen: investigation of the CD8 expression by a subpopulation of dendritic cells. *J Exp Med* 1992;176:47–58.
37 Durrant DM, Robinette ML, Klein RS. Il-1R1 is required for dendritic cell-mediated T cell reactivation within the CNS during West Nile virus encephalitis. *J Exp Med* 2013;210:503–16.
38 Jia B, Zhao C, Rakszawski KL, *et al*. $Eomes^+T\text{-}bet^{low}$ $CD8^+$ T cells are functionally impaired and are associated with poor clinical outcome in patients with acute myeloid leukemia. *Cancer Res* 2019;79:1635–45.
39 Qiu Z, Khairallah C, Romanov G, *et al*. Cutting edge: Batf3 expression by CD8 T cells critically regulates the development of memory populations. *J.i.* 2020;205:901–6.
40 Tsuda M, Hamade H, Thomas LS, *et al*. A role for BATF3 in Th9 differentiation and T-cell-driven mucosal pathologies. *Mucosal Immunol* 2019;12:644–55.
41 Yamamoto TN, Kishton RJ, Restifo NP. Developing neoantigen-targeted T cell–based treatments for solid tumors. *Nat Med* 2019;25:1488–99.
42 Grenier JM, Yeung ST, Qiu Z, *et al*. Combining adoptive cell therapy with Cytomegalovirus-Based vaccine is protective against solid skin tumors. *Front Immunol* 2017;8:1–10.
43 Ma L, Dichwalkar T, Chang JYH, *et al*. Enhanced CAR-T cell activity against solid tumors by vaccine boosting through the chimeric receptor. *Science* 2019;365:162–8.
44 Laoui D, Keirsse J, Morias Y, *et al*. The tumour microenvironment harbours ontogenically distinct dendritic cell populations with opposing effects on tumour immunity. *Nat Commun* 2016;7:13720.
45 Rafiq S, Yeku OO, Jackson HJ, *et al*. Targeted delivery of a PD-1-blocking scFv by CAR-T cells enhances anti-tumor efficacy in vivo. *Nat Biotechnol* 2018;36:847–56.
46 Miller BC, Sen DR, Al Abosy R, *et al*. Subsets of exhausted $CD8^+$ T cells differentially mediate tumor control and respond to checkpoint blockade. *Nat Immunol* 2019;20:326–36.
47 Kurtulus S, Madi A, Escobar G, *et al*. Checkpoint blockade immunotherapy induces dynamic changes in PD-1–CD8+ tumor-infiltrating T cells. *Immunity* 2019;50:181–94.

48 Curnis F, Sacchi A, Borgna L, *et al*. Enhancement of tumor necrosis factor α antitumor immunotherapeutic properties by targeted delivery to aminopeptidase N (CD13). *Nat Biotechnol* 2000;18:1185–90.
49 Reina M, Espel E. Role of LFA-1 and ICAM-1 in cancer. *Cancers* 2017;9:153–14.
50 Kammertoens T, Friese C, Arina A, *et al*. Tumour ischaemia by interferon-γ resembles physiological blood vessel regression. *Nature* 2017;545:98–102.
51 Platzer C, Meisel C, Vogt K, *et al*. Up-Regulation of monocytic IL-10 by tumor necrosis factor-α and cAMP elevating drugs. *Int Immunol* 1995;7:517–23.

Supplementary Materials for

Selective IL-1 activity on CD8$^+$ T cells empowers antitumor immunity and synergizes with neovasculature-targeted TNF for full tumor eradication

Bram Van Den Eeckhout, Leander Huyghe, Sandra Van Lint, Elianne Burg, Stéphane Plaisance, Frank Peelman, Anje Cauwels, Gilles Uzé, Niko Kley, Sarah Gerlo* and Jan Tavernier*

*Corresponding authors. Email: sarah.gerlo@ugent.be and jan.tavernier@vib-ugent.be

These Supplementary Materials include:

- Supplementary Figures and Table Legends
- Supplementary Figures 1 – 16
- Supplementary Table 1 – 2
- Supplementary Methods
- Supplementary References

Van Den Eeckhout B, *et al. J Immunother Cancer* 2021; 9:e003293. doi: 10.1136/jitc-2021-003293

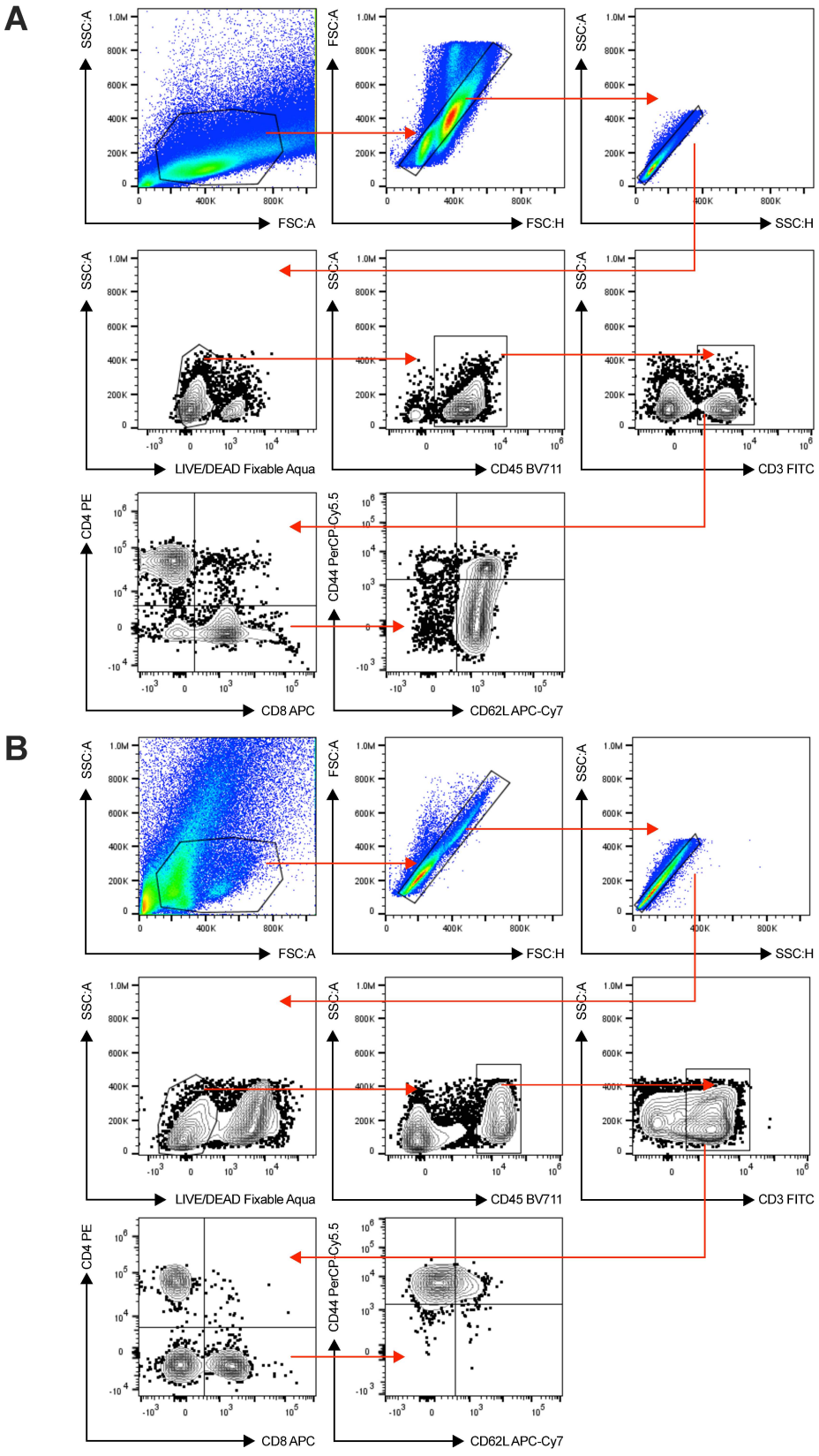
A
SSC:A
FSC:A
FSC:A
FSC:H
SSC:A
SSC:H
LIVE/DEAD Fixable Aqua
CD45 BV711
CD3 FITC
CD4 PE
CD8 APC
CD44 PerCP-Cy5.5
CD62L APC-Cy7
B
SSC:A
FSC:A
FSC:A
FSC:H
SSC:A
SSC:H
LIVE/DEAD Fixable Aqua
CD45 BV711
CD3 FITC
CD4 PE
CD8 APC
CD44 PerCP-Cy5.5
CD62L APC-Cy7

Supplementary Figure 1. Gating strategy for the detection of naive and effector $CD8^+$ T cells in the TDLN (**A**) and tumor tissue (**B**) of LLC-OVA tumor-bearing mice via flow cytometry. Staining with LIVE/DEAD Fixable Aqua cell viability dye, CD45 BV711, CD3 FITC, CD4 PE, CD8 APC, CD44 PerCP-Cy5.5 and CD62L APC-Cy7. In the living ($LIVE/DEAD^-$) subset of single cells (based on FSC/SSC), we detected naive $CD8^+$ T cells as $CD45^+CD3^+CD4^-CD8^+CD44^-CD62L^+$ cells and effector $CD8^+$ T cells as $CD45^+CD3^+CD4^-CD8^+CD44^+CD62L^-$ cells.

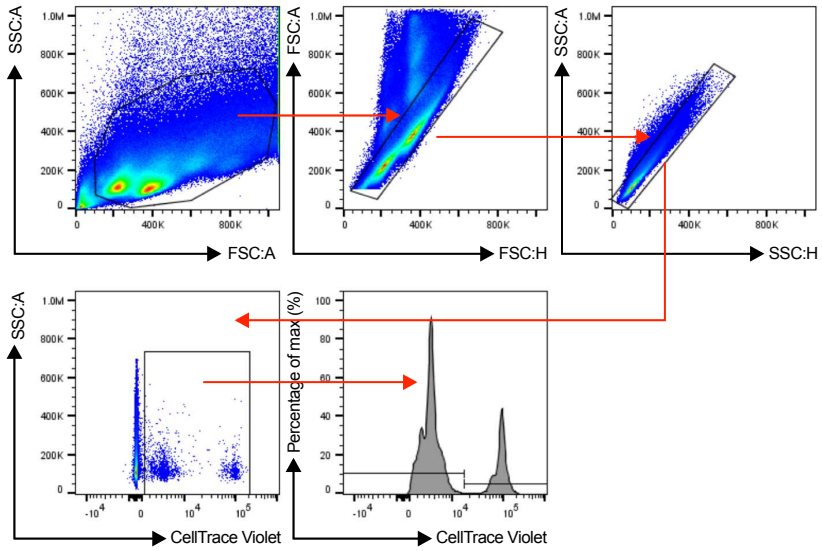

Supplementary Figure 2. Gating strategy for the detection of adoptively transferred target cells in the spleens of acceptor mice. Prior to transfer, cells were labeled with CTV in a high or low concentration and loaded with SIINFEKL (CTV^{high}) or left unloaded (CTV^{low}).

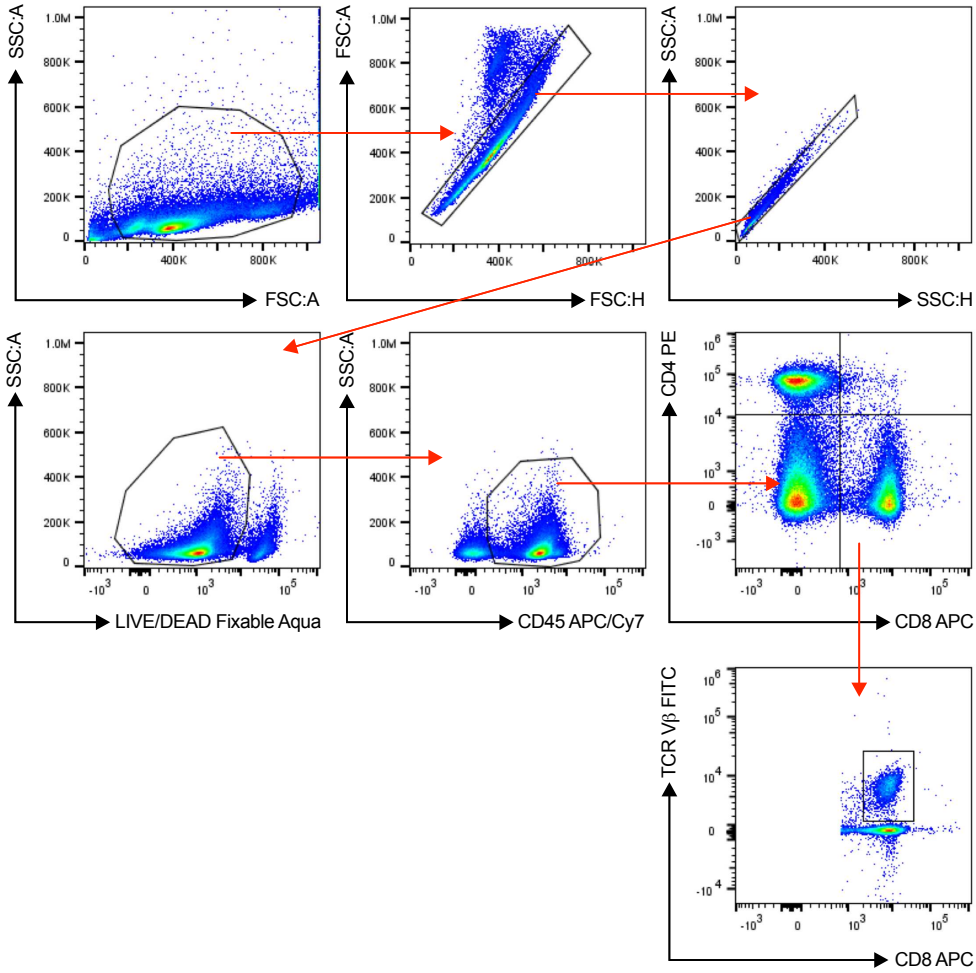

Supplementary Figure 3. Gating strategy for the detection of different TCR Vβ clonotypes in the TDLN of LLC-OVA tumor-bearing mice via flow cytometry. Staining with LIVE/DEAD Fixable Aqua cell viability dye, CD45 APC-Cy7, CD4 PE, CD8 APC and different TCR Vβ FITC antibodies. Clonotype frequencies were measured in the $CD45^{+}CD4^{-}CD8^{+}$ and $CD45^{+}CD4^{+}CD8^{-}$ subsets of living ($LIVE/DEAD^{-}$) single cells (based on FSC/SSC).

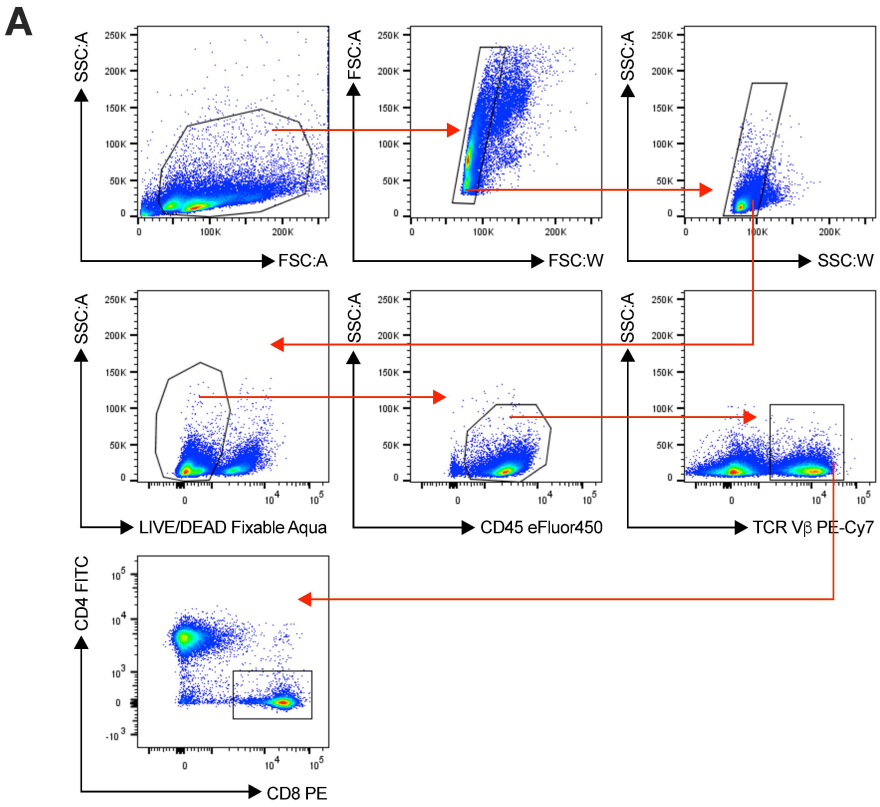
A
SSC:A
FSC:A
FSC:A
FSC:W
SSC:A
SSC:W
SSC:A
LIVE/DEAD Fixable Aqua
SSC:A
CD45 eFluor450
SSC:A
TCR Vβ PE-Cy7
CD4 FITC
CD8 PE

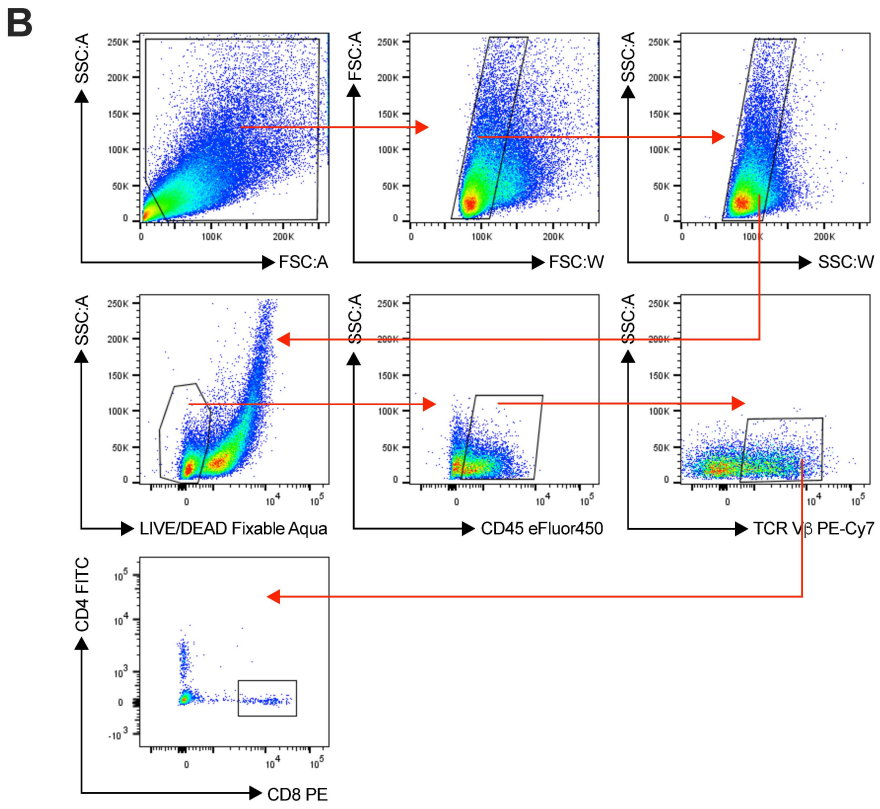
B
SSC:A
FSC:A
FSC:A
FSC:W
SSC:A
SSC:W
SSC:A
LIVE/DEAD Fixable Aqua
SSC:A
CD45 eFluor450
SSC:A
TCR Vβ PE-Cy7
CD4 FITC
CD8 PE

Supplementary Figure 4. Gating strategy for the sort of $CD8^+$ T cells from the TDLN (**A**) and tumor tissues (**B**) of LLC-OVA tumor-bearing mice. Staining with LIVE/DEAD Fixable Aqua cell viability dye, CD45 eFluor450, TCR Vβ PE-Cy7, CD4 FITC and CD8 PE. In the living ($LIVE/DEAD^-$) subset of single cells (based on FSC/SSC), we detected $CD8^+$ T cells as $CD45^+TCR\ V\beta^+CD4^-CD8^+$ cells.

Van Den Eeckhout B, *et al. J Immunother Cancer* 2021; 9:e003293. doi: 10.1136/jitc-2021-003293

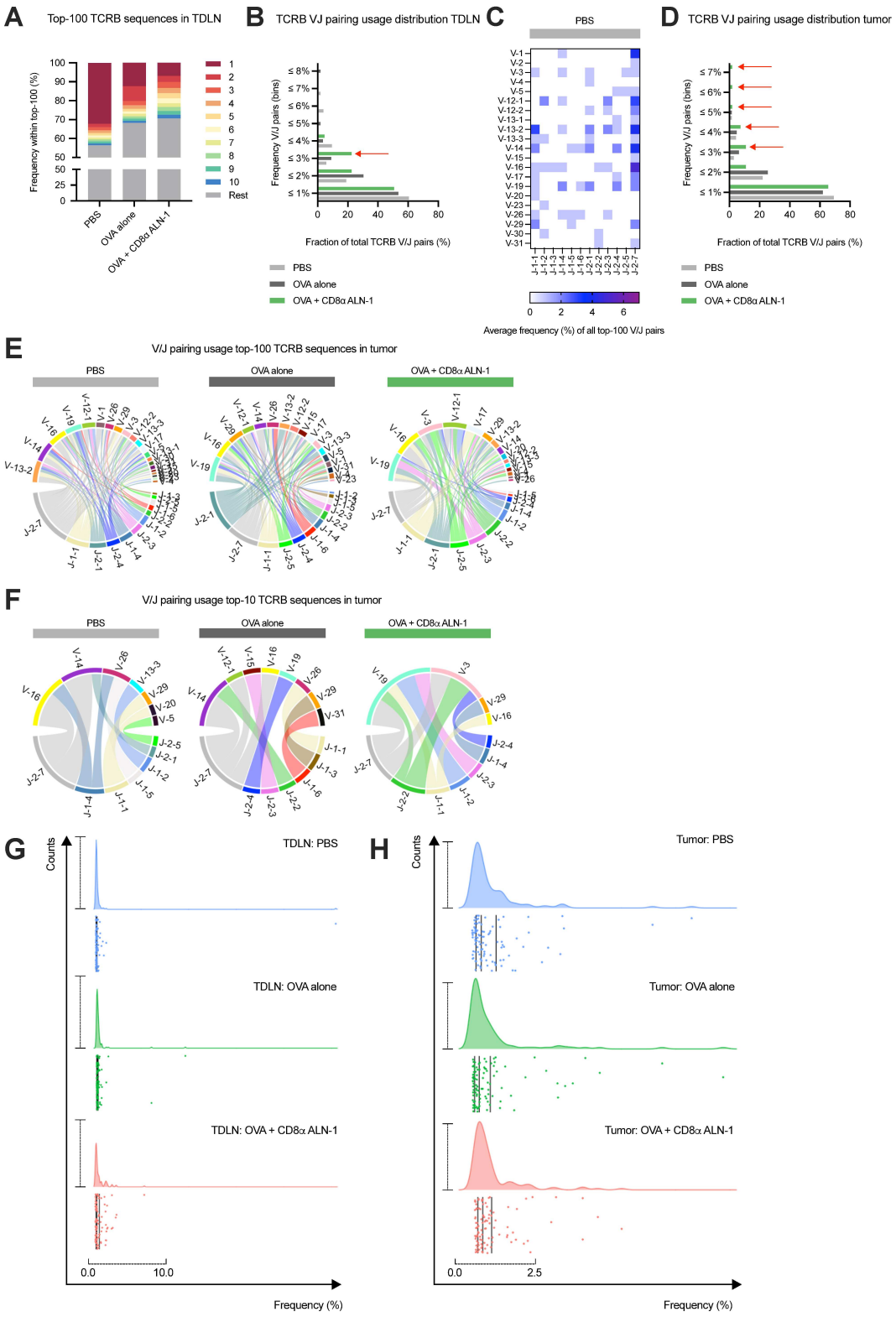
A
Top-100 TCRB sequences in TDLN
Frequency within top-100 (%)
PBS
OVA alone
OVA + CD8α ALN-1
Rest
B
TCRB VJ pairing usage distribution TDLN
Frequency VJ pairs (bins)
Fraction of total TCRB V/J pairs (%)
C
PBS
Average frequency (%) of all top-100 V/J pairs
D
TCRB VJ pairing usage distribution tumor
E
V/J pairing usage top-100 TCRB sequences in tumor
F
V/J pairing usage top-10 TCRB sequences in tumor
G
TDLN: PBS
TDLN: OVA alone
TDLN: OVA + CD8α ALN-1
Counts
Frequency (%)
H
Tumor: PBS
Tumor: OVA alone
Tumor: OVA + CD8α ALN-1

Supplementary Figure 5. (**A**) Frequency of the top-10 most abundant TCRB sequences (stacked bars in color) within the top-100 most abundant TDLN TCRB sequences. The same color does not necessarily represent the same clonotype in the different bars. Data from individual mice were pooled per group. (**B**) **and** (**D**) Frequency distribution of V/J pairing usage of the top-100 most abundant TCRB sequences in the TDLN (**B**) and tumor (**D**). (**C**) V/J pairing usage within the top-100 most abundant TDLN TCRB sequences for mice treated with PBS. (**E**) **and** (**F**) V/J pairing usage within the top-100 (**E**) and top-10 (**F**) most abundant tumor TCRB sequences. (**G**) **and** (**H**) Frequency distribution of the top-100 most abundant TCRB sequences in TDLN (**G**) and tumor (**H**). Histograms (*top*) give an overview of the frequency distribution per group with dotted lines indicating the scale for both axes. Points *(bottom)* represent the individual clones that comprise the top-100 TCRB sequences. Black vertical lines represent Q1, Q2 (= median) and Q3.

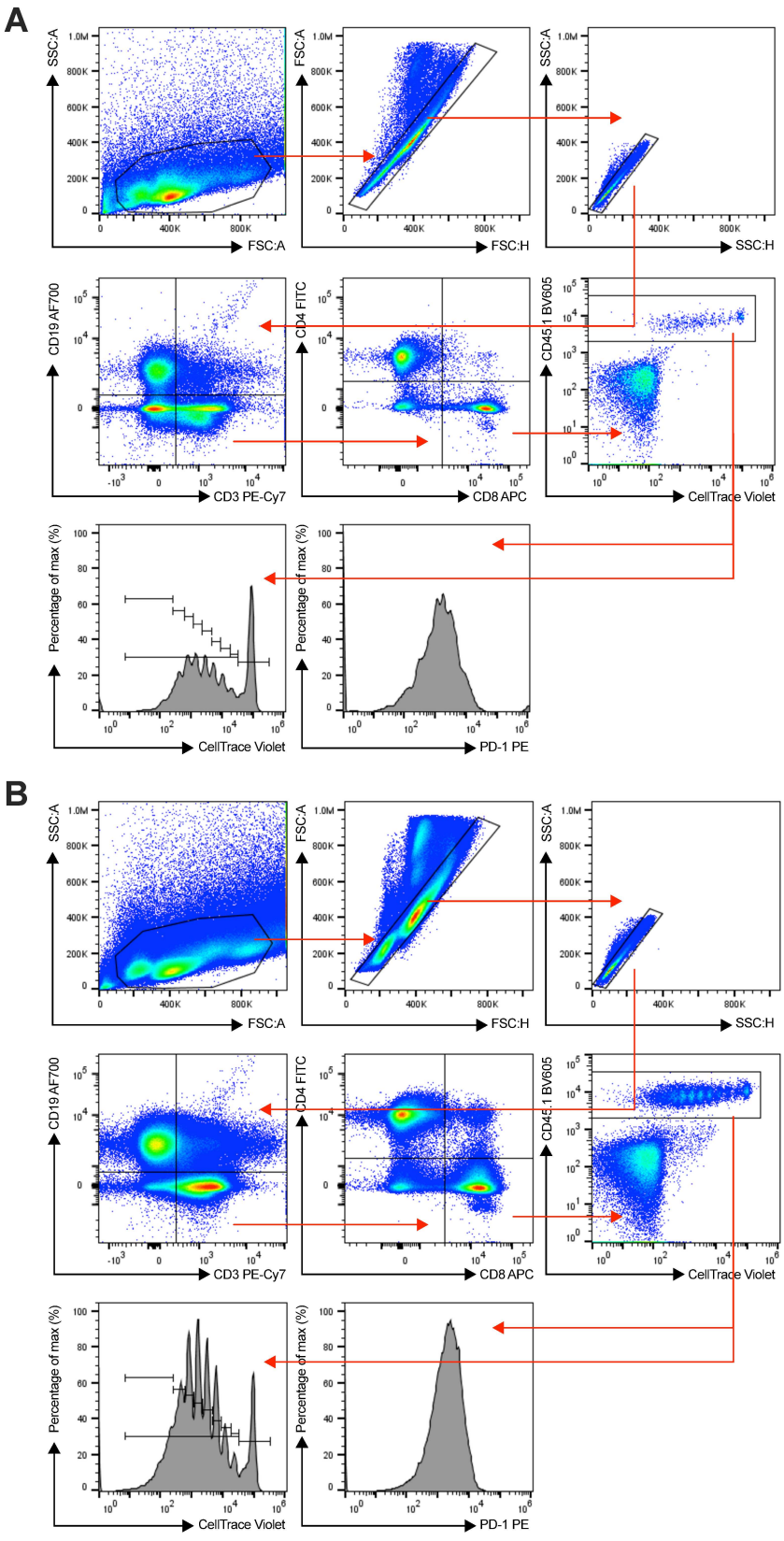
A
SSC:A
FSC:A
FSC:A
FSC:H
SSC:A
SSC:H
CD19 AF700
CD3 PE-Cy7
CD4 FITC
CD8 APC
CD45.1 BV605
CellTrace Violet
Percentage of max (%)
CellTrace Violet
Percentage of max (%)
PD-1 PE
B
SSC:A
FSC:A
FSC:A
FSC:H
SSC:A
SSC:H
CD19 AF700
CD3 PE-Cy7
CD4 FITC
CD8 APC
CD45.1 BV605
CellTrace Violet
Percentage of max (%)
CellTrace Violet
Percentage of max (%)
PD-1 PE

Supplementary Figure 6. Gating strategy for the detection of OT-I $CD8^+$ T cell proliferation and PD-1 upregulation in the TDLNs of B16- (**A**) and LLC-OVA (**B**) tumor-bearing mice via flow cytometry. Staining with CD19 AF700, CD3 PE-Cy7, CD4 FITC, CD8 APC and CD45.1 BV605. OT-I $CD8^+$ T cells were detected as $CD19^-CD3^+CD4^-CD8^+CD45.1^+CTV^{labeled}$ cells within the single cell population (based on FSC/SSC).

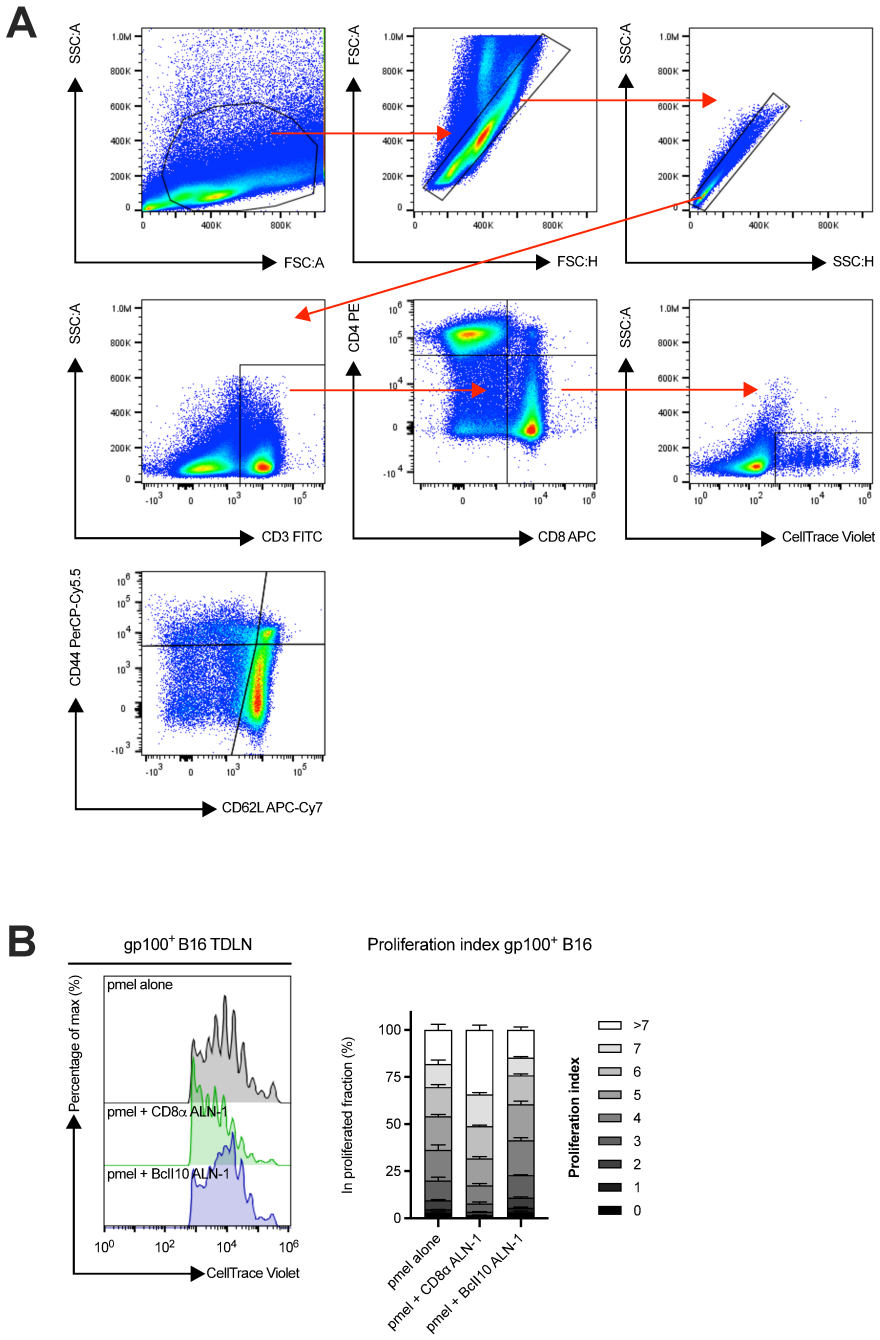

Supplementary Figure 7. (**A**) Gating strategy for the detection of pmel $CD8^+$ T cell proliferation in the TDLNs of B16 $gp100^+$ tumor-bearing mice via flow cytometry. Staining with CD3 FITC, CD4 PE and CD8 APC. pmel $CD8^+$ T cells were detected as $CD3^+CD4^-CD8^+CTV^{labeled}$ cells within the single cell population (based on FSC/SSC). (**B**) Stacked

histograms summarizing the proliferation index of pmel $CD8^+$ T cell proliferation in B16 $gp100^+$ tumor-bearing mice. Individual stacks represent the mean percentages of proliferating pmel $CD8^+$ T cells in certain stages of cell division ± s.e.m. of an experiment with $n = 6$ mice/group. Representative flow cytometry histograms display pmel $CD8^+$ T cell proliferation.

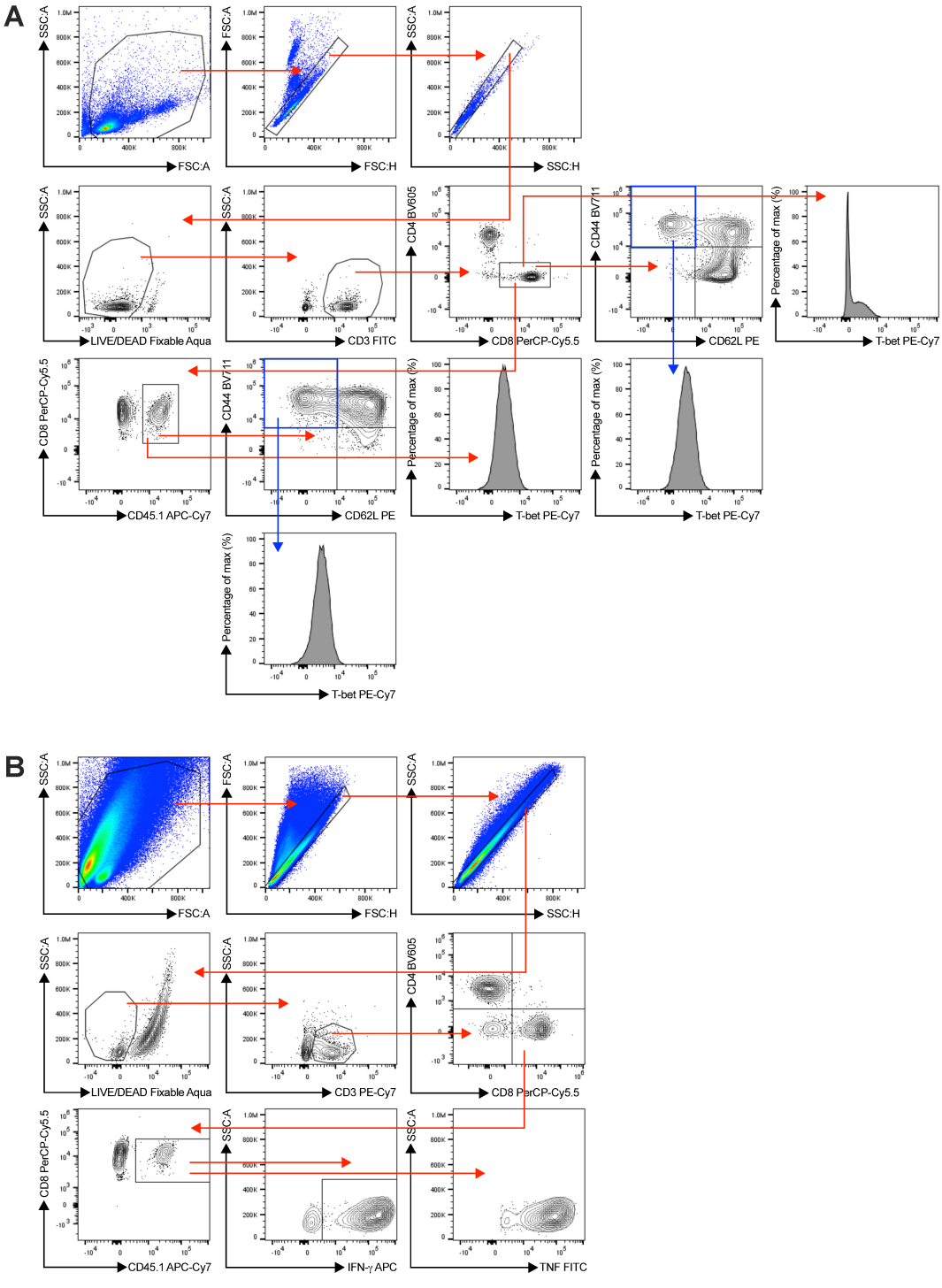

Supplementary Figure 8. (**A**) Gating strategy for the detection of naive and effector (OT-I) $CD8^+$ T cells in the TDLN and tumor tissue of LLC-OVA tumor-bearing mice. Staining with

LIVE/DEAD Fixable Aqua cell viability dye, CD3 FITC, CD4 BV605, CD8 PerCP-Cy5.5, CD45.1 APC-Cy7, CD44 BV711, CD62L PE and T-bet PE-Cy7. Naive and effector (OT-I) $CD8^+$ T cells were identified within the living ($LIVE/DEAD^-$) single cell (based on FSC/SSC) population as $CD3^+CD4^-CD8^+(CD45.1^+)CD44^-CD62L^+$ cells and $CD3^+CD4^-CD8^+(CD45.1^+)CD44^+CD62L^-$ cells, respectively. (**B**) Gating strategy for the detection of cytokine release following *ex vivo* restimulation of murine splenocytes with SIINFEKL peptide. Staining with LIVE/DEAD Fixable Aqua cell viability dye, CD3 PE-Cy7, CD4 BV605, CD8 PerCP-Cy5.5, CD45.1 APC-Cy7, IFN-γ APC and TNF FITC. We detected IFN-γ and TNF release in the $CD3^+CD4^-CD8^+(CD45.1^+)$ cells within the population of living ($LIVE/DEAD^-$) single cells (based on FSC/SSC).

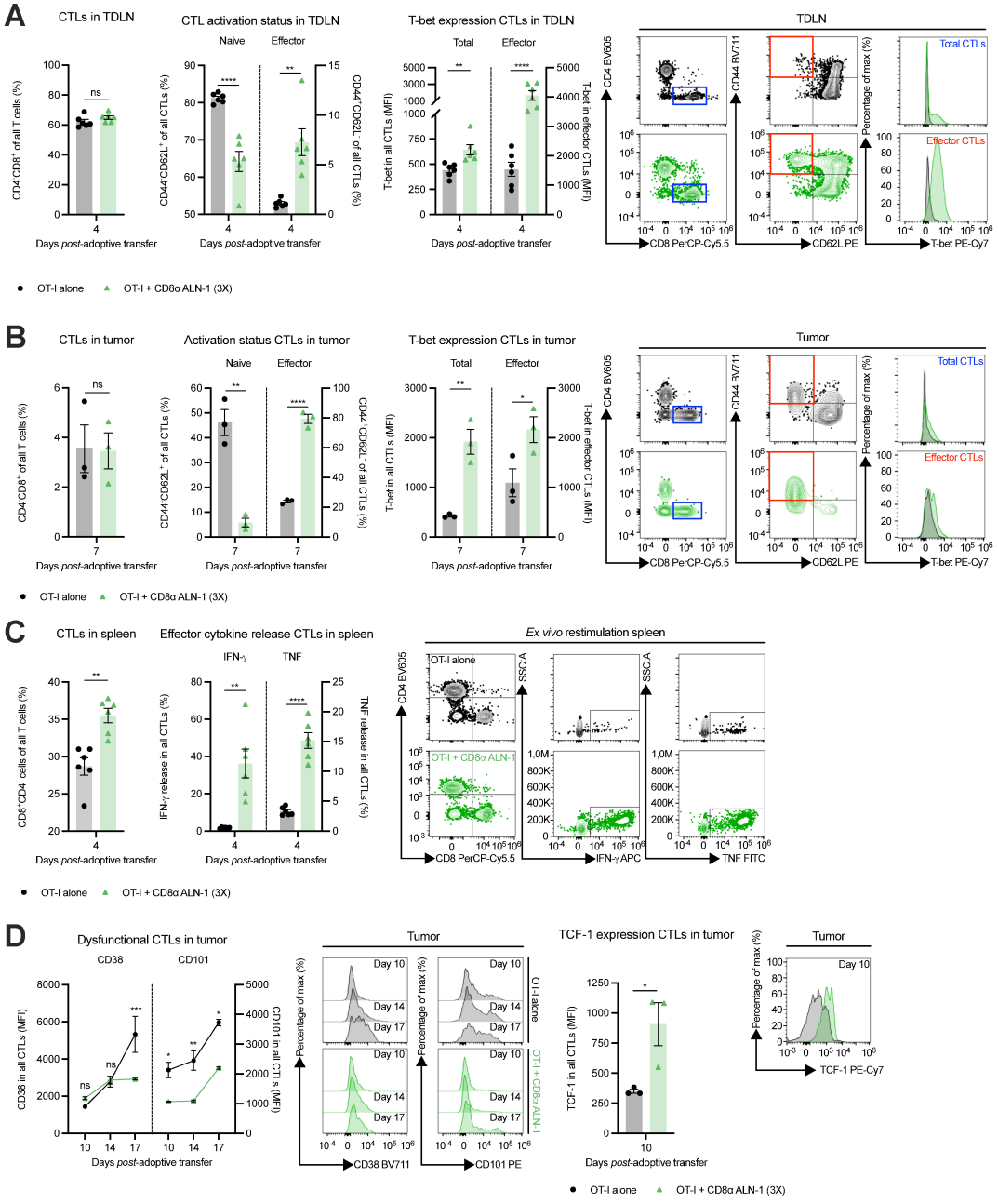

Supplementary Figure 9. (**A**) **and** (**B**) Frequencies of CD8$^+$ T cells within the total T cell population, naive (CD44$^-$CD62L$^+$) and effector (CD44$^+$CD62L$^-$) phenotypes within the total CD8$^+$ T cell population and T-bet expression within the total and effector CD8$^+$ T cell population in TDLN (**A**) and tumor tissue (**B**) with representative flow cytometry dot plots. (**C**) Frequencies of CD8$^+$ T cells within the total T cell population and release of IFN-γ and

TNF by $CD8^+$ T cells following *ex vivo* restimulation of splenocytes with SIINFEKL peptide with representative flow cytometry dot plots. (**D**) Expression of CD101, CD38 and TCF-1 on $CD8^+$ T cells in tumor with representative flow cytometry histograms. Bars and data points represent the mean ± s.e.m. of an experiment with $n = 6$ mice/group (for TDLN and spleen samples) or $n = 3$ mice/group (for tumor samples, as two mice were pooled together). ****, $p < 0.0001$; ***, $p < 0.001$; **, $p < 0.01$; *, $p < 0.05$; ns, $p \geq 0.05$ by unpaired Student's *t*-test (**A – D**) or two-way ANOVA with Sidak's multiple comparison's test (**D**).

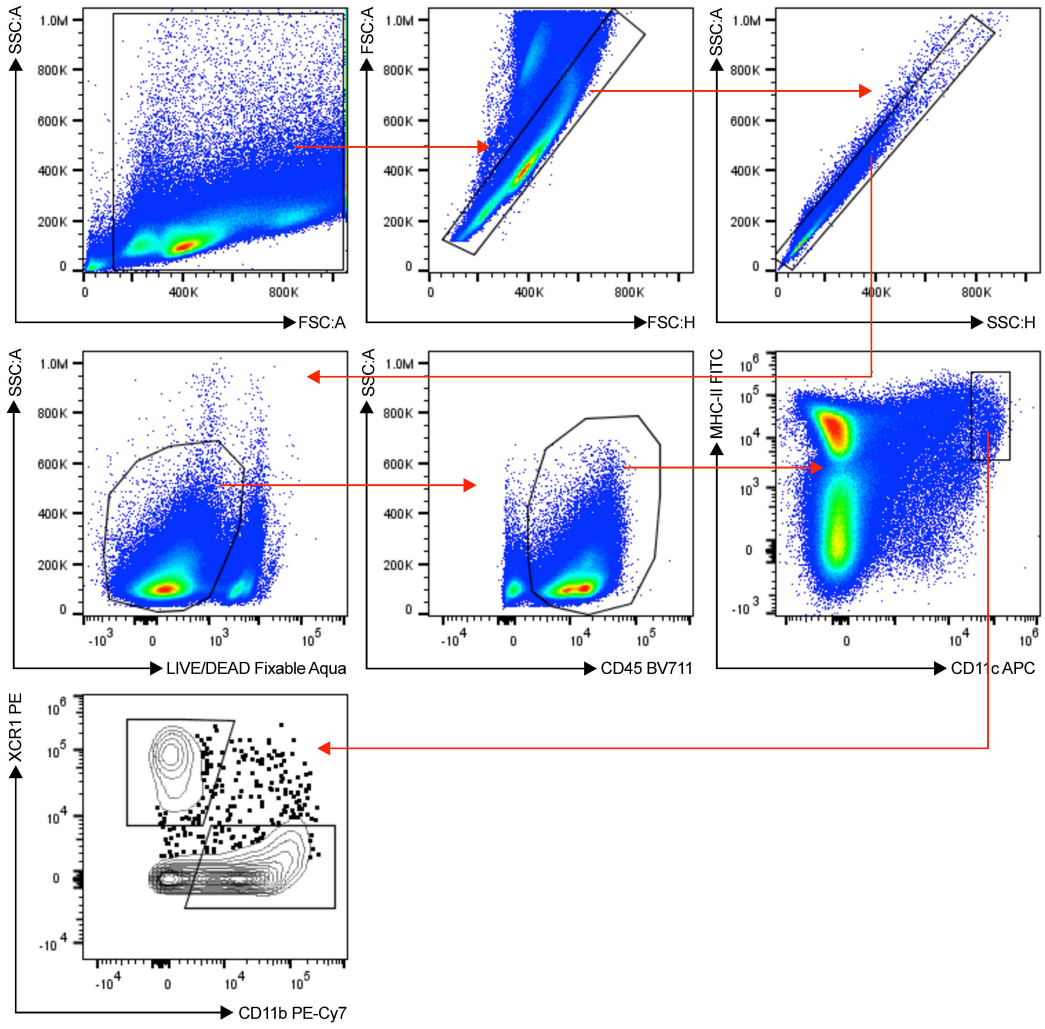

Supplementary Figure 10. Gating strategy for the detection of cDC1s and cDC2 in the TDLNs of LLC-OVA tumor-bearing mice via flow cytometry. Staining with LIVE/DEAD Fixable Aqua cell viability dye, CD45 BV711, MHC-II FITC, CD11c APC, XCR1 PE and CD11b PE-Cy7. Within the subset of living (LIVE/DEAD$^-$) single cells (based on FSC/SSC), we detected cDC1s as CD45$^+$MHC-II$^+$CD11c$^+$XCR1$^+$CD11b$^-$ cells and cDC2 as CD45$^+$MHC-II$^+$CD11c$^+$XCR1$^-$CD11b$^+$ cells.

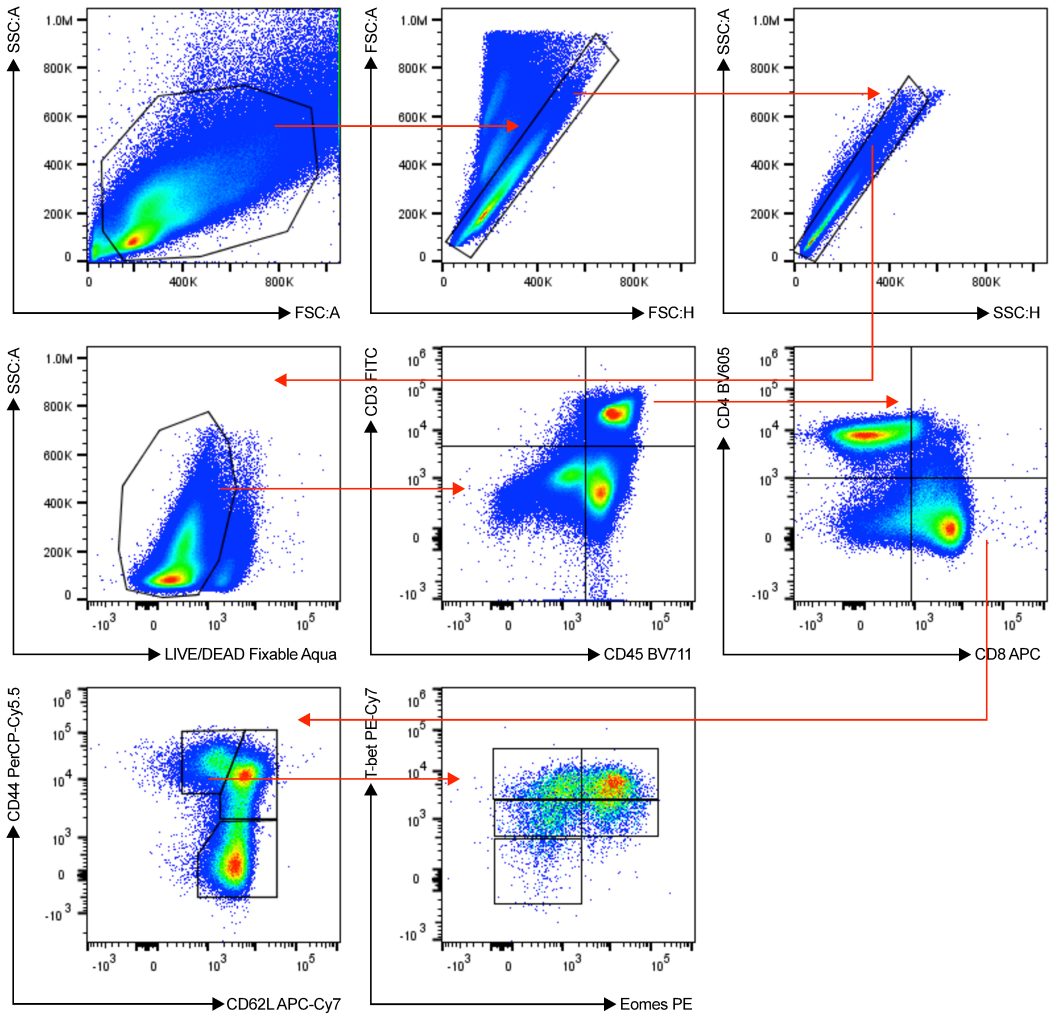

Supplementary Figure 11. Gating strategy for the detection of naive and effector CD8$^+$ T cells in the TDLNs of WT or full-body Batf3$^{-/-}$ C57BL/6 mice. Staining with LIVE/DEAD

Fixable Aqua cell viability dye, CD3 FITC, CD45 BV711, CD4 BV605, CD8 APC, CD44 PerCP-Cy5.5, CD62L APC-Cy7, T-bet PE-Cy7 and Eomes PE. In the living (LIVE/DEAD$^-$) subset of single cells (based on FSC/SSC), we detected naive CD8$^+$ T cells as CD45$^+$CD3$^+$CD4$^-$CD8$^+$CD44$^-$CD62L$^+$ cells and effector CD8$^+$ T cells as CD45$^+$CD3$^+$CD4$^-$CD8$^+$CD44$^+$CD62L$^-$ cells.

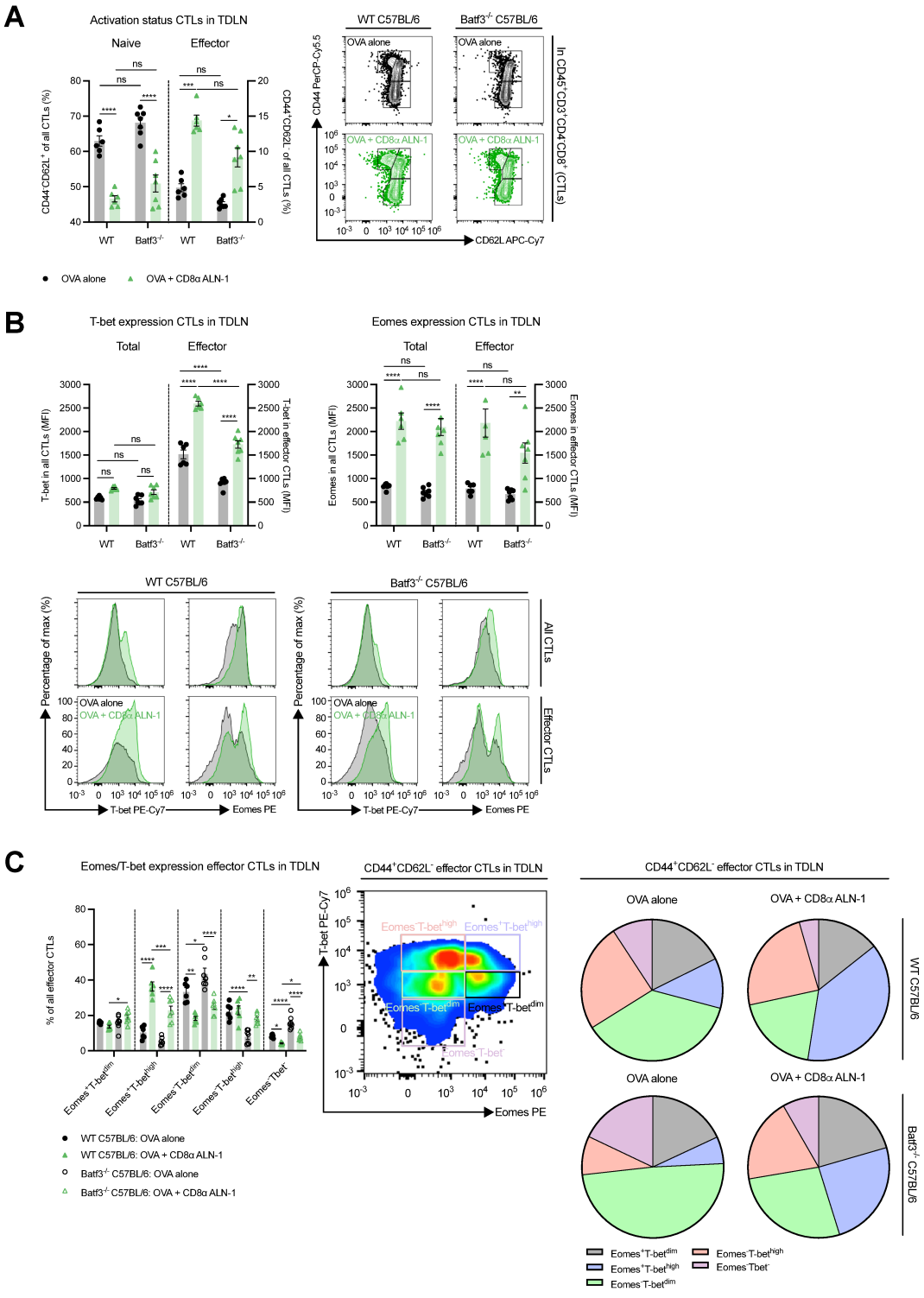

Supplementary Figure 12. (**A**) Relative amounts of naive ($CD44^{-}CD62L^{+}$) and effector ($CD44^{+}CD62L^{-}$) $CD8^{+}$ T cells within the total CTL population in TDLNs of WT or full-body

Batf3$^{-/-}$ LLC-OVA tumor-bearing mice (*left*) with representative flow cytometry dot plots (*right*). (**B**) Expression (MFI) of T-bet and Eomes in the total or effector CD8^{+} T cell population in TDLNs of WT or full-body Batf3$^{-/-}$ LLC-OVA tumor-bearing mice (*top*) with representative flow cytometry histograms (*bottom*). (**C**) Relative amounts of different T-bet/Eomes-expressing effector CD8^{+} T cell populations within TDLNs of WT or full-body Batf3$^{-/-}$ LLC-OVA tumor-bearing mice (*left*) according to the gating strategy displayed in the representative flow cytometry dot plot (*middle*). Fractions of the different T-bet/Eomes-expressing effector CD8^{+} T cell population represented as parts-of-whole (*right*). Bars represent the mean ± s.e.m. of an experiment with $n = 6$ mice/group. ****, $p < 0.0001$; ***, $p < 0.001$; **, $p < 0.01$; *, $p < 0.05$; ns, $p \geq 0.05$ by one-way ANOVA with Tukey's multiple comparisons test.

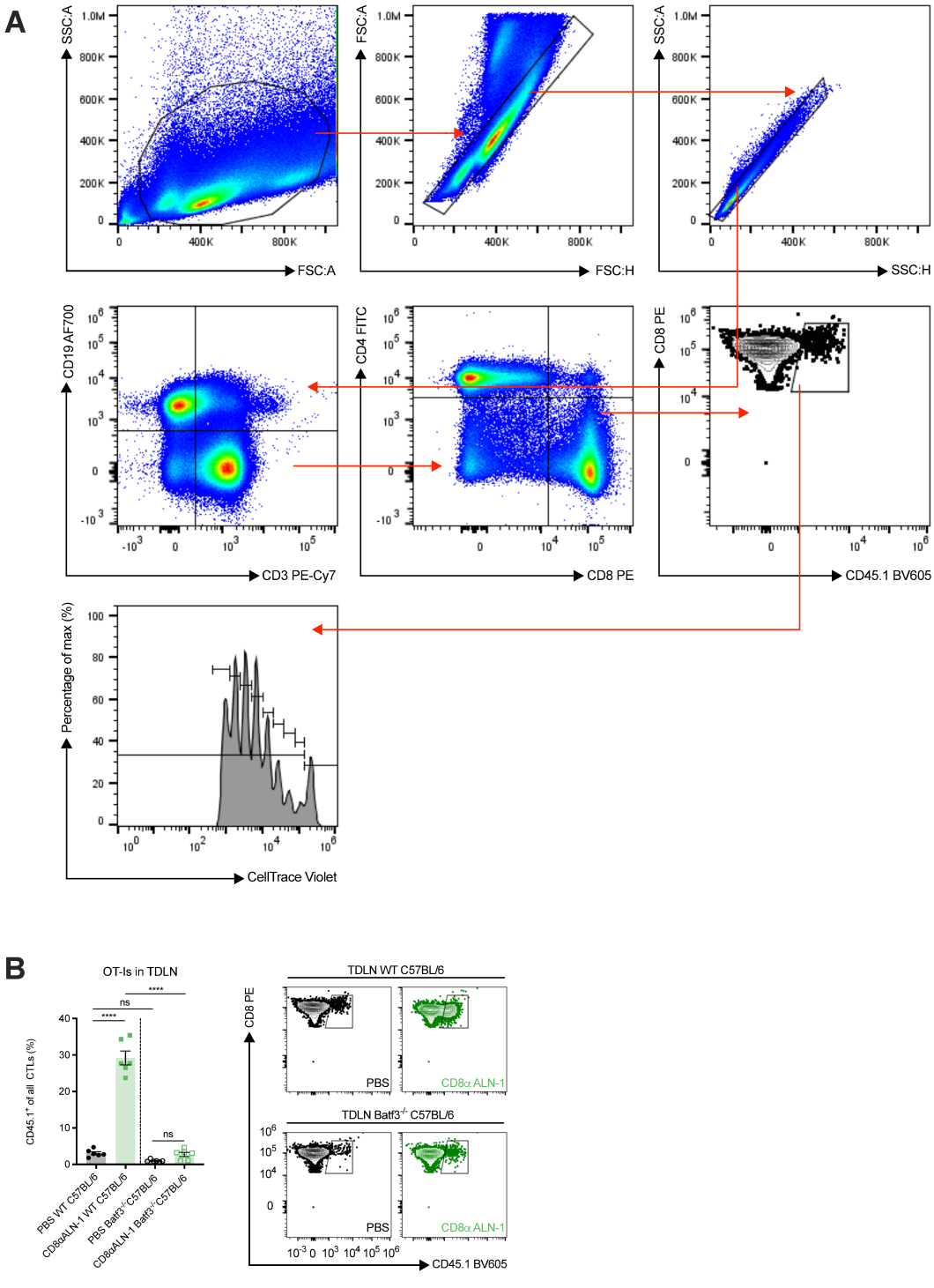

Supplementary Figure 13. (**A**) Gating strategy for the detection of OT-I $CD8^+$ T cell proliferation in the TDLNs of WT or full-body $Batf3^{-/-}$ C57BL/6 mice. Staining with CD19

AF700, CD3 PE-Cy7, CD4 FITC, CD8 PE and CD45.1 BV605. OT-I $CD8^+$ T cells were detected as $CD19^-CD3^+CD4^-CD8^+CD45.1^+$ cells within the single cell population (based on FSC/SSC) and proliferation was measured as CTV dilution. (**B**) Relative amounts of OT-I $CD8^+$ T cells within the total $CD8^+$ T cell population in TDLNs of WT and full-body $Batf3^{-/-}$ LLC-OVA tumor-bearing acceptor mice (*left*) with representative flow cytometry dot plots (*right*). Bars represent the mean ± s.e.m. of an experiment with $n = 6$ mice/group. ****, $p < 0.0001$; ns, $p \geq 0.05$ by one-way ANOVA with Tukey's multiple comparisons test.

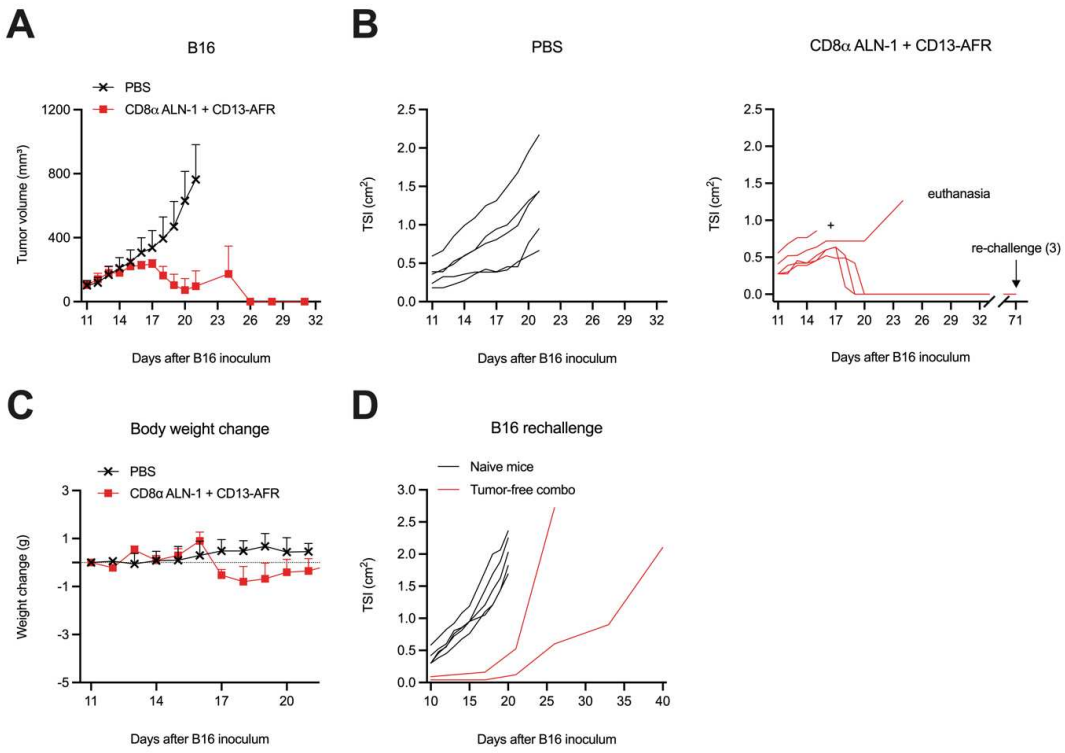

Supplementary Figure 14. Mice were inoculated with B16 ($0.6x10^6$ cells) and treatment was initiated after 10 days of s.c. tumor growth. From D10 – D13, mice received an i.p. treatment with CD8α ALN-1 (10 μg) combined with additional i.p. treatments with CD13 AFR (50 μg) from D14 – D16. Control mice received i.p. treatments with PBS from D10 – D16. (**A**) B16 tumor growth over time. Data points represent the mean ± s.e.m. of one experiment with $n = 5$

mice/group. (**B**) B16 tumor growth over time for the individual treatment conditions. Individual mice are shown. (**C**) Change in body weight over time. Data points represent the mean ± s.e.m. of one experiment with $n = 5$ mice/group. (**D**) B16 tumor growth over time after s.c. rechallenge of mice previously treated with CD8α ALN-1 + CD13 AFR. Naive mice were used as control animals in this experiment. Individual mice are shown.

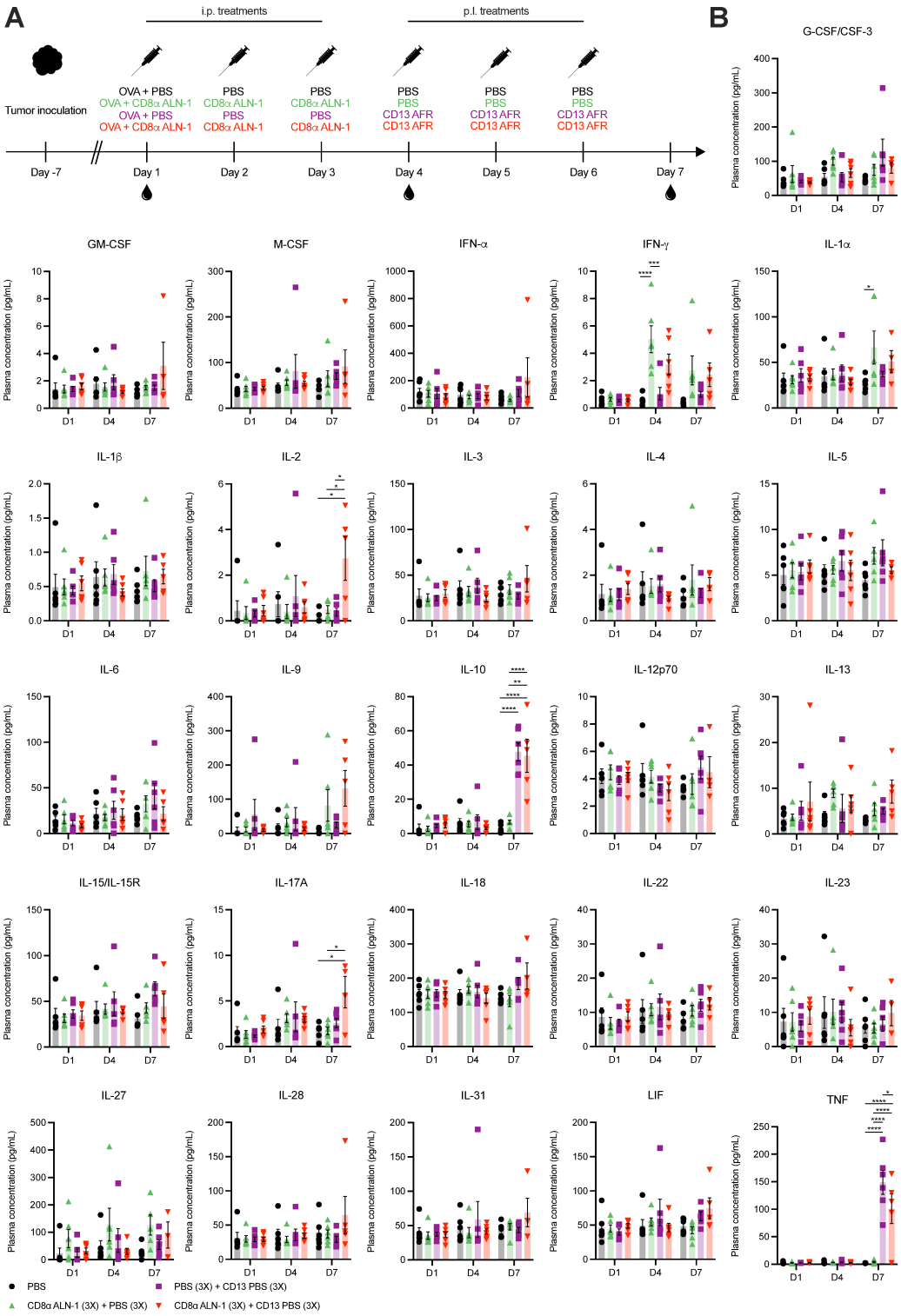
A
i.p. treatments
p.i. treatments
Tumor inoculation
OVA + PBS
OVA + CD8α ALN-1
OVA + PBS
OVA + CD8α ALN-1
PBS
CD8α ALN-1
PBS
CD8α ALN-1
PBS
CD8α ALN-1
PBS
CD13 AFR
PBS
CD13 AFR
PBS
CD13 AFR
PBS
PBS
PBS
CD13 AFR
PBS
CD13 AFR
Day -7
Day 1
Day 2
Day 3
Day 4
Day 5
Day 6
Day 7
B
G-CSF/CSF-3
GM-CSF
M-CSF
IFN-α
IFN-γ
IL-1α
IL-1β
IL-2
IL-3
IL-4
IL-5
IL-6
IL-9
IL-10
IL-12p70
IL-13
IL-15/IL-15R
IL-17A
IL-18
IL-22
IL-23
IL-27
IL-28
IL-31
LIF
TNF
Plasma concentration (pg/mL)
D1
D4
D7
PBS
PBS (3X) + CD13 PBS (3X)
CD8α ALN-1 (3X) + PBS (3X)
CD8α ALN-1 (3X) + CD13 PBS (3X)

Supplementary Figure 15. (**A**) Schematic representation of the experiment. LLC-OVA tumors were grown s.c. for seven days, after which mice received i.p. treatments with OVA (100 μg) in combination with PBS or CD8α ALN-1 (10 μg) every 24h for three consecutive days, followed by p.l. treatments with PBS or CD13 AFR (50 μg) every 24h for three consecutive days. Tail vein blood was sampled at the start of treatment (day 1), the fourth day of treatment (day 4) or one day after the last treatment (day 7). (**B**) Plasma cytokine concentrations following different treatments over time. Bars represents the mean ± s.e.m. of an experiment with $n = 6$ mice/group. ****, $p > 0.0001$; ***, $p > 0.001$; **, $p > 0.01$; *, $p > 0.05$; ns, $p \geq 0.05$ by one-way ANOVA with Tukey's multiple comparisons test.

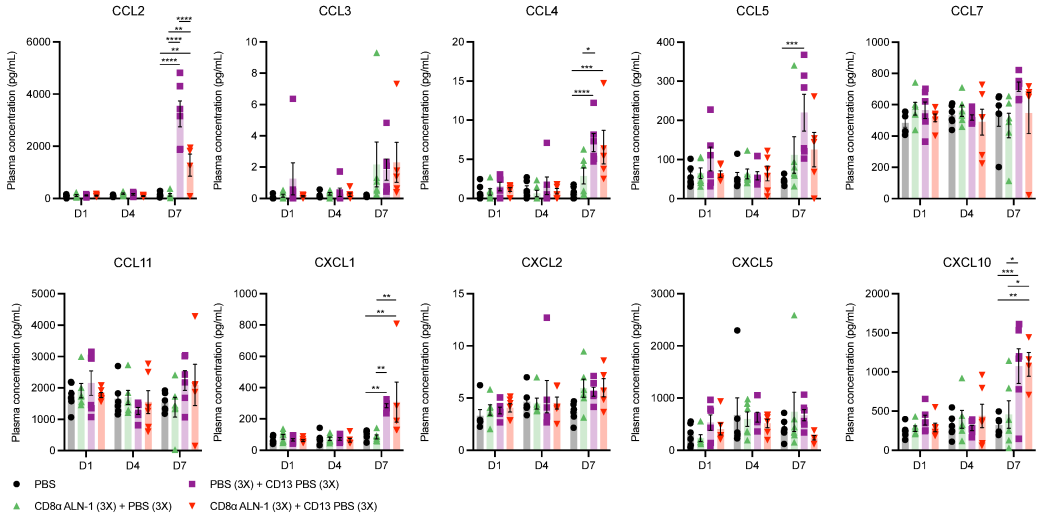

Supplementary Figure 16. Plasma chemokine concentrations following different treatments over time. Bars represents the mean ± s.e.m. of an experiment with $n = 6$ mice/group. ****, $p > 0.0001$; ***, $p > 0.001$; **, $p > 0.01$; *, $p > 0.05$; ns, $p \geq 0.05$ by one-way ANOVA with Tukey's multiple comparisons test.

Target and fluorochrome	Dilution	Clone	Category number	Supplier
CD16/32	100	clone 93	14-0161-82	Thermo Fisher Scientific
CD19 AF700	500	clone 145-2C11	552774	BD Biosciences
CD4 FITC	250	clone RM4-5	100510	BioLegend
CD8 APC	250	clone 53-6.7	553035	BD Biosciences
CD8 PE	250	clone 53-6.7	12-0081-82	Thermo Fisher Scientific
CD45.1 BV605	250	clone A20	110737	BioLegend
PD-1 PE	100	clone J43	12-9985-82	Thermo Fisher Scientific
LIVE/DEAD Fixable Aqua cell viability dye	1000		L34957	Thermo Fisher Scientific
CD45 BV711	500	clone 30-F11	103147	BioLegend
CD3 FITC	250	clone 17A2	555274	BD Biosciences
CD4 PE	250	clone RM4-5	553048	BD Biosciences
CD4 BV605	250	clone RM4-5	100547	BioLegend
CD44 PerCP-Cy5.5	100	clone IM7	103032	BioLegend
CD62L APC-Cy7	100	clone MEL-14	104428	BioLegend
T-bet PE-Cy7	100	clone 4B10	644823	BioLegend
Eomes PE	100	clone Dan11mag	12-4875-82	Thermo Fisher Scientific
MHC-II FITC	250	clone M5/114.15.2	11-5321-82	Thermo Fisher Scientific
CD11c APC	250	clone N418	117310	BioLegend
XCR1 PE	100	clone ZET	148204	BioLegend
CD11b PE-Cy7	250	clone M1/70	101215	BioLegend
CD40 Pacific Blue	100	clone 3/23	124626	BioLegend
CD86 APC-Cy7	100	clone GL-1	105030	BioLegend
CD45 APC-Cy7	500	clone 30-F11	103116	BioLegend
TCR Vb FITC (15 clonotypes)			557004	BD Biosciences
CD45 eFluor450	500	clone 30-F11	48-0451-82	Thermo Fisher Scientific
TCR Vb PE-Cy7	250	clone KT11	125916	BioLegend
CD8 PerCP-Cy5.5	250	clone 53-6.7	100733	BioLegend
CD44 BV711	100	clone IM7	103057	BioLegend
CD62L PE	100	clone MEL-14	104407	BioLegend
CD45.1 APC-Cy7	250	clone A20	560579	BD Biosciences
CD38 BV711	100	clone 90/CD38	740697	BD Biosciences
CD101 PE	100	clone Moushi101	12-1011-82	Thermo Fisher Scientific
TCF-1 PE-Cy7	100	clone C63D9	90511	Cell Signaling Technology
IFN-g APC	100	clone XMG1.2	562019	BD Biosciences
TNF FITC	100	clone MP6-XT22	506303	BioLegend

Supplementary Table 1. Complete list of antibodies and dyes used in this manuscript.

TCR clonotype	OVA alone group	OVA + CD8α ALN-1 group	Change compared with OVA alone
Vβ2	4,928333333	5,046666667	0,118333333
Vβ3	2,77	2,83	0,06
Vβ4	3,675	3,746666667	0,071666667
Vβ5.1/2	13,06666667	11,93333333	-1,133333333
Vβ6	6,658333333	6,406666667	-0,251666667
Vβ7	5,843333333	5,828333333	-0,015
Vβ8.1/2	15,61666667	15,33333333	-0,283333333
Vβ8.3	6,46	6,528333333	0,068333333
Vβ9	1,883333333	2,331666667	0,448333333
Vβ10b	4,938333333	5,143333333	0,205
Vβ11	5,085	6,043333333	0,958333333
Vβ12	2,541666667	2,518333333	-0,023333333
Vβ13	3,648333333	3,952	0,303666667
Vβ14	2,548333333	2,853333333	0,305
Vβ17b	0,82	0,505	-0,315
Others	19,51666667	18,99966667	-0,517

Supplementary Table 2. Average frequencies and change in average frequencies of $CD8^+$ TCR Vβ clonotypes. Mice were treated with OVA alone or OVA + CD8α ALN-1 according to the treatment scheme presented in Fig. 4A (n = 6 mice/group).

Supplementary Methods

Recombinant protein design, production and purification

Site-directed mutagenesis was used to introduce the Q148G and Y86F mutation in the coding sequence of human IL-1β and murine TNF, respectively[1,2]. Generation and selection of sdAbs was performed by the VIB Protein Service Facility[1–3]. Proteins were constructed in an in-house developed vector, produced in mammalian FreeStyleTM 293-F cells (R79007, Thermo Fisher Scientific) and purified from supernatants as described elsewhere[1]. Purity was evaluated by SDS-PAGE and Instant Blue (EP ISB1L, Expedeon) staining of the protein gel.

Cell lines and culture conditions

B16- and LLC-OVA cells (Damya Laoui, VIB-VUB) were cultured in DMEM (41966-052, Thermo Fisher Scientific) or RPMI-1640 (61870-044, Thermo Fisher Scientific) + 10% fetal bovine serum (FBS) (10270-106, Thermo Fisher Scientific). All cell lines were grown at 37°C in a humidified atmosphere containing 5% CO_2 and tested negative for mycoplasma (Venor^{TM}GeM Mycoplasma Detection Kit, PCR-based, MP0025, Sigma-Aldrich). We did not perform full authentication of the cell lines.

Mice

Female C57BL/6 mice were purchased from Charles River Laboratories. OT-I TCR transgenic CD45.1 Rag2$^{-/-}$ C57BL/6 mice (Bart Lambrecht, VIB-UGent) and full-body Batf3$^{-/-}$ C57BL/6 mice (Karine Breckpot, VUB) were bred in our facility. All mice were housed under pathogen-free conditions in IVCs and temperature-controlled environments with a 12h day/12h night cycle and received food and water *ad libitum*. FELASA guidelines were followed in all experiments and approval was obtained by the Ethical Committee of the Faculty of Medicine and Health Sciences (UGent) (ECD 17/80k, ECD 18/127k and ECD 16/07). Mice were

randomly allocated to treatments and investigators were not blinded during data collection and analysis.

Formulae

Tumor volumes (mm^3) were calculated as: [longest perpendicular side (mm) x shortest perpendicular side (mm) x shortest perpendicular side (mm)]/2. The percentage of SIINFEKL-specific cytolytic activity was calculated as: $100-[100 \times (\%CTV^{high}$ treated mice/$\%CTV^{low}$ treated mice)/($\%CTV^{high}$ PBS-treated mice/$\%CTV^{low}$ PBS-treated mice)].

TCR sequencing, data processing and analysis (detail)

Briefly, RNA was reverse transcribed into cDNA with TCR-specific RT primers. Double-stranded cDNA was generated via second-strand synthesis, after which cDNA was end-repaired and A-tailed. Every original cDNA molecule was assigned a unique molecular identifier (UMI) by ligation of a 12-base random adaptor sequence. Target enrichment was performed via PCR with one primer against the constant region and another primer complementary to the adapter. The library was ultimately amplified via a second PCR, which also introduced platform-specific adaptor sequences and additional sample indices. Samples were then pooled and sequenced in two Illumina MiSeq v2 500 runs. The read data was merged and analyzed using the mouse "Immune Repertoire Analysis" workflow of the CLC Genomics Workbench (GWB) v21 (https://digitalinsights.qiagen.com/)[4]. The analysis was done using default parameters, except for "min UMI group size", which was set to 1. The obtained clonotype results were used to produce count tables and figures.

Statistical analyses and data presentation (detail)

Data sets were compared by unpaired Student's *t*-testing (two-tailed) for the statistical analysis of differences between two groups or ANOVA (one- or two-way) with Tukey's or Sidak's multiple comparisons test for the statistical analysis of differences between more than two

groups. Statistical analysis of differences between Kaplan–Meier survival curve was performed by log-rank testing.

Supplementary References

1. Van Den Eeckhout, B. *et al.* Specific targeting of IL-1β activity to CD8+ T cells allows for safe use as a vaccine adjuvant. *npj Vaccines* **5**, 1–17 (2020).

2. Huyghe, L. *et al.* Safe eradication of large established tumors using neovasculature-targeted tumor necrosis factor-based therapies. *EMBO Mol. Med.* **12**, 1–15 (2020).

3. Garcin, G., Paul, F., Staufenbiel, M., Bordat, Y. & Van der Heyden, J. High efficiency cell-specific targeting of cytokine activity. *Nat. Commun* **5**, 1–9 (2014).

4. Bolotin, D. A. *et al.* MiXCR: software for comprehensive adaptive immunity profiling. *Nature Methods* vol. 12 380–381 (2015).

Selective IL-1 activity on CD8⁺ T cells empowers antitumor immunity and synergizes with neovasculature-targeted TNF for full tumor eradication

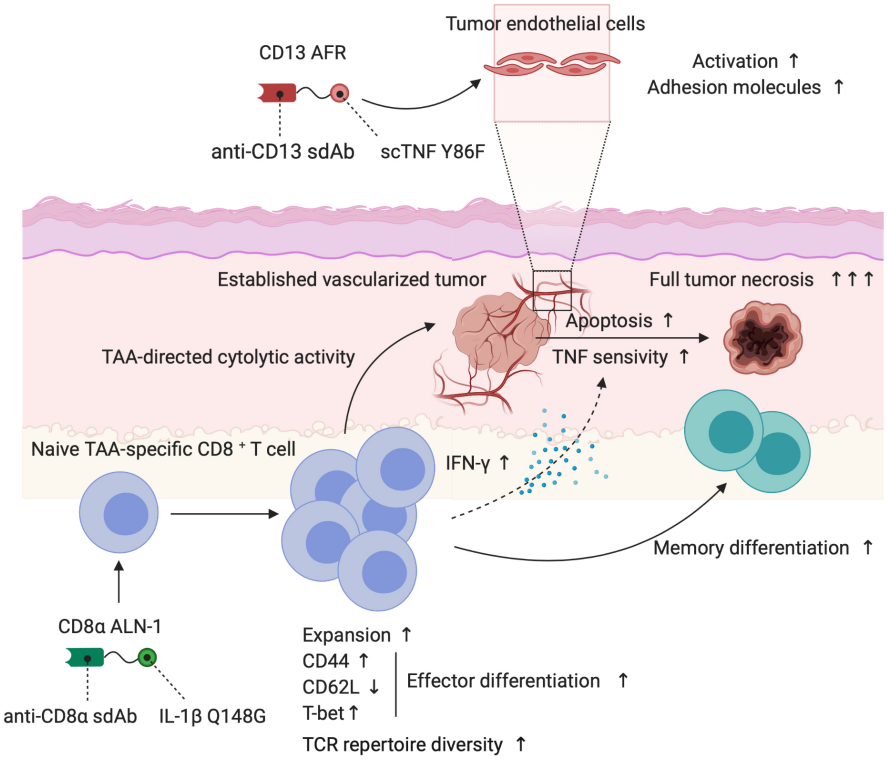

Authors
Bram Van Den Eeckhout, Leander Huyghe, Sandra Van Lint, Elianne Burg, Stéphane Plaisance, Frank Peelman, Anje Cauwels, Gilles Uzé, Niko Kley, Sarah Gerlo and Jan Tavernier

Correspondence
sarah.gerlo@ugent.be
jan.tavernier@vib-ugent.be

In Brief
AcTakines represent engineered cytokines that deliver cytokine activity to selected cell types only, as such evading damaging toxicities and unwanted off-target side effects. Here, an AcTakine that targets IL-1β activity to CD8⁺ T cells safely and efficiently drives antitumor cellular immunity. Combination with a neovasculature-targeted TNF AcTakine induces full tumor necrosis and establishes a protective immunological memory.